1 **Title:**

2 Myosin II regulatory light chain phosphorylation and formin availability modulate cytokinesis upon

3 changes in carbohydrate metabolism.

4

5 **Running title:**

6 Regulation of cytokinesis during respiration.

7

8 **Authors:**

9 Francisco Prieto-Ruiz[1], Elisa Gómez-Gil[1,2], Rebeca Martín-García[3], Armando Jesús Pérez-Díaz[1], Jero

10 Vicente-Soler[1], Alejandro Franco[1], Teresa Soto[1], Pilar Pérez[3], Marisa Madrid[1]* and José Cansado[1]*

11

12 [1]Yeast Physiology Group. Department of Genetics and Microbiology. Campus de Excelencia

13 Internacional de Ámbito Regional (CEIR) Campus Mare Nostrum, Universidad de Murcia. 30071

14 Murcia, Spain.

15 [2]The Francis Crick Institute, 1 Midland Road, London, NW1 1AT, UK.

16 [3]Instituto de Biología Funcional y Genómica (IBFG), Consejo Superior de Investigaciones Científicas,

17 Universidad de Salamanca. 37007 Salamanca, Spain.

18

19 * To whom correspondence should be addressed:

20 José Cansado, Department of Genetics and Microbiology, Universidad de Murcia, 30071 Murcia, Spain.

21 Tel: +34868884953; Email: jcansado@um.es

22 Marisa Madrid, Department of Genetics and Microbiology, Universidad de Murcia, 30071 Murcia, Spain.

23 Tel: +34868887132; Email: marisa@um.es

24

25 **Author Contributions:** J.C. and M.M. supervised the study. J.C., M.M, and P.P. conceived and designed

26 the study. F.P-R., E.G-G., R.M.-G., J.C., and M.M. developed the methodology. F.P-R., E.G-G., R.M.-G.,

27 A.P.-D., J.V-S., A.F., and T.S. designed and performed experiments. F.P-R., E.G-G., R.M.-G., A.P.-D.,

28 J.V-S., A.F., T.S., P.P., M.M. and J.C. analyzed and interpreted the data. J.C., M.M, and P.P. wrote,

29 reviewed and revised the manuscript.

30

31 **Keywords:** Cytokinesis; Respiration; Myosin II; Formin; p21-activated kinase; Fission Yeast

Abstract

Cytokinesis, which achieves the separation of daughter cells after mitosis completion, relies in animal cells on a contractile actomyosin ring (CAR), made of actin and class II myosins, whose activity is heavily influenced by regulatory light chain (RLC) phosphorylation. However, in simple eukaryotes such as fission yeast *Schizosaccharomyces pombe*, regulation of CAR dynamics by RLC phosphorylation seems dispensable. We found that redundant phosphorylation at Ser35 of the *S. pombe* RLC homolog Rlc1 by the p21-activated kinases Pak1 and Pak2, modulates Myosin II Myo2 activity and becomes essential for cytokinesis and cell growth during respiration. Previously, we showed that the Stress Activated Protein Kinase Pathway (SAPK) MAPK Sty1 controls fission yeast CAR integrity by downregulating formin For3 levels (Gomez-Gil et al.,2020). Here we report that reduced availability of formin For3-nucleated actin filaments for the CAR is the main reason for the required control of myosin II contractile activity by RLC phosphorylation during respiration-induced oxidative stress. Hence, recovery of For3 levels with antioxidants bypasses the control of Myosin II function regulated by RLC phosphorylation to allow cytokinesis and cell proliferation during respiration. Therefore, a fine-tuned interplay between Myosin II function by Rlc1 phosphorylation and environmentally controlled actin filament availability is critical for a successful cytokinesis in response to a switch to a respiratory carbohydrate metabolism.

Introduction

Cytokinesis, the final step in cell division, enables the physical separation of daughter cells after mitosis has been completed [1]. In non-muscle animal cells, this process is based on the formation of a contractile actomyosin ring ('CAR'), made of actin filaments and non-muscle myosin II (NMII), which generates the mechanical force for actomyosin contractility [2, 3]. The prototype NMII motor unit is a complex assembled by two heavy chains, two light chains known as ELC (essential light chain), which provide structural integrity to the complex, and two regulatory light chains or RLC, which induce a change in NMII from a folded to an extended conformation to modulate its activity in response to phosphorylation [2]. Phosphorylation of RLC at Ser19 is critical for NMII to achieve an extended conformation, which results in the spontaneous and immediate formation of bipolar filaments with enhanced actin binding affinity and increased ATPase motor activity [2, 4, 5]. Accordingly, NMII is enzymatically inactive in the absence of RLC phosphorylation at this site [6], thus resulting in defective cytokinesis and an increase in multinucleate cells [7], which are phenotypes similar to those induced by deletion or pharmacological inhibition of NMII [8, 9]. ROCK (Rho-associated coiled-coil-containing kinase), CITK (citron kinase), and ZIPK (zipper-interacting protein kinase) are involved in NMII activation by RLC phosphorylation on Ser19 during its accumulation at the cleavage furrow, and CAR contraction, stabilization, and scission during cytokinesis [2]. RLC phosphorylation at additional sites besides Ser19, including Thr18, Ser1/2 and/or Tyr-155, provide further regulatory layers to modulate either positively or negatively the contractile activity of NMII within specific cellular conditions [2].

Schizosaccharomyces pombe, a Crabtree-positive fission yeast that can grow through either fermentative or respiratory metabolism, is a well-established model organism studying cytokinesis [10-12]. This simple eukaryote employs a CAR to achieve cellular division with two myosin-II heavy chains known as Myo2 and Myp2/Myo3 [13]. Myo2 function is essential for viability and cytokinesis during normal growth conditions, while Myp2 plays a subtle non-essential role for cytokinesis during unperturbed growth, and is specifically required for cell survival in response to saline stress [14-16]. Contrary to animal NMII, purified Myo2 does not form filaments at physiological saline concentrations, but instead adopts a unipolar organization, with the head domains exposed to the cytoplasm and its tails anchored into medial precursor nodes of the CAR during the mitotic onset [17-20]. The essential formin Cdc12 is responsible for the nucleation and elongation of actin filaments at the nodes. At early anaphase, a search, capture, pull, and release mechanism driven by Myo2 promotes the fusion of the equatorial nodes to form a mature CAR [21-23]. For3, a non-essential diaphanous-like formin that assembles actin cables for cellular transport, also plays a significant role in fission yeast cytokinesis nucleating actin filaments for CAR assembly and disassembly [24, 25]. Remarkably, in response to cytoskeletal damage

82   and environmental cues, the stress-activated signaling protein kinase pathway (SAPK), and its core

83   effector Sty1, a p38 MAPK ortholog, promotes CAR disassembly and block cell division by reducing

84   For3 levels and the availability of actin filaments [25]. Once formed, coordinated CAR constriction by

85   Myo2 and Myp2, and concomitant plasma membrane and primary septum formation at late anaphase,

86   generate the physical barriers that allow the separation of the two daughter cells [10, 13, 26].

87   Cdc4 and Rlc1 are the respective ELC and RLC shared by Myo2 and Myp2 in fission yeast [27-

88   29]. Early evidence indicated that Ser35 and Ser36 of Rlc1, which are homologous to RLC Thr18 and

89   Ser19 in NMIIs, are phosphorylated by the p21/Cdc42-activated kinase (PAK) ortholog Pak1/Shk1/Orb2

90   [30], which has also been involved in RLC phosphorylation at Ser19 in animal cells [31]. It was described

91   that Pak1-dependent phosphorylation of Rlc1 at Ser35 and Ser36 delays cytokinesis, and that expression

92   of a non-phosphorylatable mutant version at both residues (*rlc1-S35A S36A*), results in premature CAR

93   constriction [30]. These observations are consistent with *in vitro* data showing that Rlc1 phosphorylation

94   decreases the interaction of Myo2 with actin in force generation [17]. This and a later work identified

95   Ser35 as the sole target for Pak1 both *in vitro* and *in vivo* [17, 32]. On the other hand, another study

96   described that Myo2 motility is reduced in fission yeast cells expressing an *rlc1-S35A S36A* mutant

97   version, and that phosphorylation at these sites has a positive effect on CAR constriction dynamics [33].

98   Hence, while the essential role of RLC phosphorylation for NMII activity is firmly established in animal

99   cells, the biological significance of Rlc1 phosphorylation at Ser35 during fission yeast cytokinesis

100   remains currently unclear.

101   Here we show that modulation of Myo2 activity by Rlc1 phosphorylation at Ser35 is essential for

102   fission yeast cytokinesis and proliferation during respiratory growth. This posttranslational modification

103   is not only exerted by Pak1 but also by Pak2, a second PAK ortholog whose expression increases during

104   respiration. We also show that Rlc1 phosphorylation at Ser35 becomes essential due to the reduced

105   availability of For3-nucleated actin filaments caused by SAPK activation during respiration-induced

106   oxidative stress. Our findings reveal how formin-dependent actin filament nucleation and Myosin II

107   activity are linked for optimal cytokinesis control in response to changes in MAPK signaling and carbon

108   source metabolism.

109

110   **Results**

111

112   ***Myosin-II regulatory light chain phosphorylation is essential for S. pombe cytokinesis and growth***

113   ***during respiration***

114   To gain further insight into the contribution of RLC phosphorylation during Myosin II-dependent
115   control of cytokinesis in *S. pombe*, we expressed a C-terminal HA-tagged version of Rlc1 under the
116   control of its native promoter in *rlc1Δ* cells. This construct was fully functional and suppressed the
117   defects associated with the lack of Rlc1 function, including defective CAR positioning and multiseptation
118   (Figure 1—figure supplement 1A) [27]. We noted that in extracts from exponentially growing cells the
119   Rlc1-HA fusion migrates in SDS-PAGE as two discernible bands (Figure 1A). Rlc1 mobility in extracts
120   from a strain expressing a mutated version where Ser36 was changed to alanine (Rlc1(S36A)-HA) was
121   similar to the wild-type strain. In contrast, only the faster-migrating band was observed in mutants
122   expressing either Rlc1(S53A)-HA or Rlc1 (S35A S36A)-HA fusions (Figure 1A). Thus, in these assays
123   the slower motility band corresponds to the *in vivo* Rlc1 isoform phosphorylated at Ser35. Increased Rlc1
124   expression does not alter CAR integrity and/or cytokinesis in fission yeast [34]. Hence, to precisely
125   follow Rlc1 phosphorylation and localization dynamics during the cell cycle, we co-expressed Rlc1-GFP
126   (genomic fusion) and Rlc1-HA (integrative fusion) tagged versions in cells carrying an analogue-sensitive
127   version of the Cdk1 kinase ortholog Cdc2 (*cdc2-asM17*) [35], and a Pcp1-GFP fusion (pericentrin SPB
128   component; internal control for mitotic progression). Simultaneous live fluorescence microscopy and
129   Western blot analysis of synchronized cells released from the G2 arrest, showed that *in vivo* Rlc1
130   phosphorylation at Ser35 was very low at the nodes stage during CAR assembly, raised gradually during
131   ring maturation, and reached its maximum at the onset of CAR contraction until the final stages,
132   decreasing slowly during septum closure and cell separation (Figure 1B). As early suggested [30], these
133   results confirm that *in vivo* Rlc1 phosphorylation at Ser35 is enhanced during CAR constriction and
134   septum formation stages.

135   Time-lapse fluorescence microscopy of exponentially glucose-growing cells from asynchronous
136   cultures showed only a minimal but statistically significant increase in the overall time for ring
137   constriction and disassembly in Rlc1(S35A)-GFP cells as compared to wild-type Rlc1-GFP cells (18,00 $\pm$
138   3,90 *vs* 16,70 $\pm$ 2,44 min, respectively; n=92 cells) (Figure 1C). Therefore, in contrast to animal non-
139   muscle cells, where regulatory light chain phosphorylation is essential for NMII activity [2], *in vivo*
140   phosphorylation of Rlc1 has a minimal impact on myosin II function during CAR dynamics when fission
141   yeast cells grow vegetatively in the presence of glucose. These findings prompted us to search for other
142   environmental and/or nutritional condition/s where Rlc1 phoshorylation-dependent control of Myosin II
143   activity might become essential for fission yeast cytokinesis. A recent study performed with a prototroph
144   *S. pombe* deletion-mutant collection described that *rlc1Δ* cells struggle to grow in a glycerol-based
145   medium that imposes a respiratory metabolism [36]. Indeed, and in contrast to wild-type cells, the growth
146   of *rlc1Δ* cells was strongly reduced when cultured in plates with 3% glycerol and 0.08% glucose as

147 carbon sources (Figure 1D). Strikingly, cells expressing the unphosphorylated *rlc1-S35A* and *rlc1-S35A*

148 *S36A* mutants also grew very slowly in this medium (Figure 1D). This behavior was strictly dependent

149 upon Rlc1 phosphorylation at Ser35, since expression of an Rlc1-HA fusion in *rlc1Δ* cells by employing a

150 β-estradiol-regulated promoter [37], allowed their growth on glycerol only in the presence of 0.5 μM β-

151 estradiol, whereas conditional expression of the unphosphorylated Rlc1(S35A)-HA mutant version did

152 not (Figure 1—figure supplement 1B-C). Contrary to cells expressing wild-type Rlc1, the growth of *rlc1-*

153 *S35A* cells transferred to a glycerol-based liquid medium was limited to 3-4 further divisions (Figure 1E),

154 and resulted in a progressive increase in multiseptated cells with engrossed septa and lysed cells,

155 suggesting the existence of a cytokinetic defect (Figure 1E-F). Accordingly, time-lapse fluorescence

156 microscopy analysis revealed that the total time for ring assembly and disassembly in *rlc1-S35A* cells

157 incubated with glycerol for 8 hours was much longer than in those expressing wild-type Rlc1 (62,97 ±

158 6,39 *vs* 49,49 ± 4,24 min, respectively; n≥37 cells) (Figure 1G-H). The cytokinetic delay was mainly

159 observed during the stage of ring constriction and disassembly (44,29 ± 4,49 *vs* 26,84 ± 3,22 min,

160 respectively) (Figure 1G-H). The above findings support that *in vivo* Rlc1phosphorylation at Ser35 plays

161 an essential role to modulate *S. pombe* cytokinesis and cell division during respiratory growth.

162

The redundant p21/Cdc42-activated kinases Pak2 and Pak1 phosphorylate Rlc1 at Ser35 together with
to positively control fission yeast cytokinesis and division during respiratory growth

165 Earlier work has provided strong evidence that the essential fission yeast p21 (cdc42/rac)-

166 activated protein kinase (PAK) Pak1/Shk1/Orb2, phosphorylates Rlc1 at Ser35 both *in vitro* and *in vivo*

167 [30, 32]. In agreement with these studies, the *in vivo* phosphorylation of an Rlc1-HA fusion at Ser35

168 became progressively reduced in glucose-growing cells expressing the analog-sensitive (as) kinase mutant

169 Pak1-M460A treated with the specific kinase inhibitor 3-BrB-PP1, but not in the presence of the solvent

170 control (Figure 2—figure supplement 1A). Interestingly, light chain phosphorylation at Ser35 was absent

171 in glucose-growing cells expressing the hypomorphic mutant allele Pak1-M460G (Figure 2A) [30],

172 suggesting that this kinase version is constitutively inactive towards Rlc1. Unexpectedly, Rlc1 remained

173 phosphorylated at Ser35 in cells with this mutated kinase during growth with glycerol as a carbon source

174 (Figure 2A). The simplest explanation for these observations is that other kinase/s besides Pak1 can

175 specifically phosphorylate Rlc1 *in vivo* at Ser35 during respiratory growth.

176 A reasonable candidate to perform such a role is Pak2, a second PAK homolog whose over-

177 expression has been shown to restore the viability and normal morphology of fission yeast cells lacking

178 Pak1, thus suggesting that both kinases may share common substrates and functions [38, 39]. In support

179 of this hypothesis, Rlc1 phosphorylation at Ser35 was absent during respiratory growth in Pak1-M460G

pak2Δ double mutant cells, whereas it remained phosphorylated in a *pak2Δ* mutant growing with either glucose or glycerol (Figure 2A). In contrast to Pak1, Pak2 was undetectable after Western blot analysis in glucose-growing cells co-expressing genomic Pak1-GFP and Pak2-3GFP fusions (Figure 2B). However, its expression levels increased when the cells were either transferred to a medium lacking a nitrogen source or cultured with glycerol as a carbon source (Figure 2B). Enhanced Pak2-3GFP expression was also observed in glucose-rich medium as the cells reached the stationary phase of growth, when the availability of this carbohydrate is minimal (Figure 2B). Nevertheless, the relative expression of Pak2 was always very low compared to Pak1 and could only be detected after long exposure times of immunoblots (>20 min; LE; Figure 2B). Microarray-based studies have shown that *pak2$^+$* mRNA levels increase in *S. pombe* during nitrogen starvation through a mechanism that relies on Ste11, a master transcription factor that activates gene expression during the early steps of the sexual differentiation [40]. Accordingly, *pak2Δ* cells display defective fusion during mating and produce aberrant asci [41]. The *pak2$^+$* promoter shows two consecutive copies of a putative Ste11-binding motif known as the TR box (consensus sequence 5'-TTCTTTGTTY-3') (Figure 2C) [42]. Indeed, the induced expression of a Pak2-3GFP fusion during nitrogen starvation or growth with glycerol was totally abrogated in *ste11Δ* cells, and in a strain where *pak2$^+$* expression is under the control of an endogenous promoter version mutated at the two TR boxes (Figure 2C). The Zn-finger transcriptional factor Rst2, whose activity is negatively regulated by the cAMP-PKA signaling pathway in the presence of glucose, positively regulates *ste11$^+$* expression during nitrogen or glucose starvation [43]. In the presence of glucose, and in contrast to wild-type cells, Pka1 deletion prompted a constitutive increase in Pak2-GFP expression (Figure 2D). Moreover, Rst2 deletion suppressed the enhanced expression of Pak2-GFP in glucose-growing *pka1Δ* cells and in the presence of glycerol (Figure 2D). Hence, Pak2 expression is constitutively repressed by cAMP-PKA signaling during glucose fermentation and increases specifically during respiratory growth in an Rst2- and Ste11-dependent manner.

The very low expression levels of the Pak2-3GFP genomic fusion prevented the microscopic visualization of its subcellular localization during nutrient starvation. To circumvent this situation, we obtained a strain expressing a Pak2-GFP fusion under the control of the native *pak1$^+$* promoter (p^{pak1+}-Pak2-GFP). The relative expression levels of p^{pak1+}-Pak2-GFP during vegetative growth were approximately 2-3 times those of the Pak1-GFP genomic fusion (Figure 2—figure supplement 1B). Nevertheless, in contrast to Pak1-GFP, which is targeted at the cell poles and the CAR during vegetative growth with either glucose or glycerol, the p^{pak1+}-Pak2-GFP fusion localized exclusively to the CAR in both conditions (Figure 2E). Time-lapse fluorescence microscopy of glycerol-growing cells revealed that

212   Pak2 co-localized with Rlc1 during the entire cytokinetic process, starting with the early steps of CAR

213   assembly and maturation to the later stages of ring constriction (Figure 2F).

214   Compared to wild-type cells, Pak1-M460G and *pak2Δ* cells did not display cytokinetic, septation,

215   or growing defects during respiration with glycerol as a carbon source (Figure 2G-J). Strikingly, cells

216   from a Pak1-M460G *pak2Δ* double mutant showed a noticeable increase in the average time for CAR

217   assembly and disassembly (Fig 2G,H), a multiseptated phenotype (Figure 2I), and a moderated growth

218   defect in glycerol-rich medium with respect to the wild type, Pak1-M460G, and *pak2Δ* single mutants

219   (Figure 2J). Taken together, our observations support that Pak1 is fully responsible for *in vivo* Rlc1

220   phosphorylation at Ser35 during fermentative growth, whereas Pak2, whose expression is induced upon

221   nutrient starvation, collaborates with Pak1 to phosphorylate Rlc1 at this residue to regulate cytokinesis

222   during respiratory growth.

223

224   ***PAK phosphorylation of Rlc1 becomes critical for S. pombe cytokinesis during respiration due to***

225   ***impaired For3-dependent actin cable nucleation imposed by SAPK activation***

226   The formin For3 assembles actin cables for cellular transport and co-operates with the essential

227   formin Cdc12 to nucleate actin filaments for fission yeast CAR assembly and disassembly [24, 25]. For3

228   absence elicits a clear delay during ring constriction and/or disassembly in glucose-rich medium [24]. The

229   cytokinetic delay of *for3Δ* cells increased significantly in the presence of glycerol (Figure 3—figure

230   supplement 1A), and, similar to the *rlc1-S35A* mutant (Figure 1E-F), led to the accumulation of

231   multiseptated and lysed cells and a marked growth defect (Figure 3—figure supplement 1B-D), These

232   observations support that actin cable nucleation by For3 is a crucial factor ensuring proper cytokinesis

233   and growth of *S. pombe* cells during respiratory metabolism.

234   Glucose limitation or absence causes the activation of Sty1, a p38 MAPK ortholog, and the

235   critical effector of the fission yeast SAPK pathway [44]. We have recently shown that activated Sty1

236   down-regulates CAR assembly and stability in *S. pombe* in response to cytoskeletal damage and

237   environmental stress by reducing For3 levels [25]. Notably, the transfer of exponentially growing cells

238   co-expressing genomic Sty1-HA and For3-3GFP fusions from a glucose-rich medium to a medium with

239   glycerol, induced a rise in Sty1 activity that was maintained over time, as measured by Western blot

240   analysis with anti-phospho-p38 antibody, and a concomitant decrease in For3-3GFP protein levels (Figure

241   3A). Similar to environmental stresses [25], the drop in For3 levels observed during growth in glycerol is

242   likely associated with increased ubiquitination of the formin, since it was attenuated in cells of the

243   temperature-sensitive proteasome mutant *mts3-1* (Figure 3—figure supplement 1E). We used

244   immunofluorescence microscopy of cells stained with AlexaFluor-488-phalloidin, and calculated the

245   number and density of actin cables by computing the cable-to-patch ratio via image segmentation using

246   the machine learning routine Ilastik [45]. As shown in Figure 3B, the actin cable/patch ratio was

247   significantly lower in wild-type cells growing with glycerol than in those growing with glucose as carbon

248   source. The actin patches also appeared partially depolarized and their density increased during growth

249   with glycerol (Figure 3B). Fluorescence intensity at the cell poles and the CAR of a CRIB-3GFP probe

250   that detects explicitly the activated state of Cdc42 GTPase, which triggers For3 activation *in vivo* [46],

251   was also decreased under respiratory growth conditions (Figure 3—figure supplement 2A-B).

252   Accordingly, the overall intensity of a For3-3GFP fusion at the cell poles (G2 cells), and the CAR (late M

253   cells), was reduced during respiratory growth as compared to glucose-fermenting cells (Figure 3B).

254   In sharp contrast to wild-type cells (Figure 3A), we observed that the total levels of a

255   constitutively active genomic version of this formin (For3(DAD)−2GFP)[46] were not reduced in

256   response to Sty1 activation during growth with glycerol (Figure 3C). Cells expressing this Sty1-

257   insensitive For3 allele displayed engrossed actin cables with an increased actin cable to patch ratio

258   (Figure 3D-E), and required a shorter time for CAR assembly and disassembly as compared to the wild

259   type (Figure 3F-G). Most importantly, the simultaneous expression of the *for3-DAD* allele in *rlc1-S35A*

260   cells suppressed to a large extent their altered cable organization (Figure 3D-E), cytokinetic delay and

261   multiseptated phenotype (Figure 3F-I), and defective growth in glycerol-rich medium (Figure 3J). The

262   expression of *for3-DAD* also significantly abrogated the cytokinetic and growth defects in glycerol of a

263   Pak1-M460G *pak2Δ* double mutant (Figure 3F-J), which lacks detectable *in vivo* phosphorylation of Rlc1

264   at Ser35 (Figure 2A). Together, these observations indicate that For3 and PAK-phosphorylated Rlc1 may

265   perform a collaborative role during cytokinesis that becomes biologically significant when *S. pombe* cells

266   grow through a respiratory metabolism.

267   In line with our previous observations [25], total For3-GFP levels increased in glucose-growing

268   *wis1Δ* or *rlc1-S35A wis1Δ* strains lacking the Sty1-activating MAPKK Wis1[47] (Figure 4A), and

269   remained significantly higher than in the Sty1-activated isogenic counterparts during growth with glycerol

270   (Figure 4A). Similar to the *sty1Δ* mutant [25], *wis1Δ* cells growing in glycerol showed engrossed actin

271   cables and an increase in the actin cable to patch ratio per cell with respect to the wild type (Figure 4B-

272   C). Significantly, Wis1 deletion increased the actin cable to patch ratio in Rlc1-S35A-GFP cells (Figure

273   4B-C), strongly suppressed their delayed cytokinesis and multiseptation (Figure 4D-G), and restored their

274   growth in glycerol-rich medium to a large extent (Figure 4H). Phosphorylation of Rlc1 at Ser35 has a

275   minimal biological impact on *S. pombe* CAR dynamics during glucose fermentation (Figure 1C). Our

276   results predict that a constitutive increase in Sty1 activity should elicit cytokinetic defects in glucose-

277   growing *rlc1-S35A* cells. In agreement with this view, *rlc1-S35A* cells lacking the MAPK tyrosine

278 phosphatase Pyp1, which display increased basal Sty1 activity and reduced For3 levels [25], underwent a
279 significant delay in the time for CAR assembly and closure (Figure 4I-J), and accumulated septated cells
280 during stationary phase (Figure 4K-L). Therefore, tight control of Rlc1 function by phosphorylation at
281 Ser35 becomes essential for *S. pombe* cytokinesis when the levels of For3 formin are reduced by activated
282 SAPK pathway.

283

284 ***Control of Myo2 activity by Rlc1 phosphorylation regulates S. pombe cytokinesis and growth during***
285 ***respiration***

286 The thermo-sensitive and motor-deficient Myosin II heavy chain allele *myo2-E1* carries a
287 mutation (G345R), that results in reduced ATPase activity and actin-filament binding *in vitro* [13]. We
288 observed that the deficient growth in glycerol of *rlc1-S35A* cells was also displayed by *Myo2-E1* cells, but
289 not by those expressing a hypomorphic allele of the essential Myosin II light chain Cdc4 (*cdc4-8*) or in a
290 mutant lacking Myp2, a second Myosin II heavy chain that collaborates with Myo2 for CAR constriction
291 during growth and saline stress [13, 16, 48] (Figure 5A). Accordingly, the time for CAR assembly and
292 disassembly was much longer in *myo2-E1* cells incubated at a semi-restrictive temperature (2 h at 30ºC),
293 and changed to the permissive temperature in a glycerol-based medium as compared to glucose-rich
294 conditions (78,59 $\pm$ 11,09 *vs* 61,67 $\pm$ 7,56 min, respectively) (Figure 5B-C). Although the respiration-
295 induced cytokinetic delay was evident during both stages of CAR assembly/maturation and ring
296 constriction/disassembly, it was more intense during the latter stages of ring closure (Figure 5B-C).
297 Similar to *rlc1-S35A* cells, the *Myo2-E1* cytokinetic defect also resulted in the accumulation of many
298 lysed and multiseptated cells with engrossed septa (Figure 5D-E). On the contrary, the delay in CAR
299 closure displayed by glucose-growing *myp2Δ* cells *versus* wild-type cells (~7.5 min; n≥37 cells), was very
300 similar to that observed during growth in glycerol (~7.7 min; n≥65 cells) (Figure 5—figure supplement
301 1A). Myp2 deletion increased the number of septated and multiseptated cells during growth in glucose
302 and, particularly, in the presence of glycerol. This phenotype was aggravated when combined with the
303 *rlc1-S35A* allele (Figure 5—figure supplement 1B).

304 Expression of the *for3-DAD* allele alleviated the altered cable organization (Figure 5F-G), and
305 reduced the cytokinetic delay of *myo2-E1* cells during CAR assembly/maturation and ring
306 constriction/disassembly (Figure 5H-I), as well as their multiseptated phenotype (Figure 5J). Moreover,
307 simultaneous expression of *for3-DAD* restored the growth of *myo2-E1* cells in glucose- and glycerol
308 media at semi-restrictive temperatures (Figure 5K). On the other hand, either *myo2-E1 rlc1-S35A* and
309 *myo2-E1 wis1Δ* double mutants were synthetic lethal. Therefore, specific regulation of myosin II heavy
310 chain Myo2 function by Pak1/Pak2-dependent *in vivo* phosphorylation of Rlc1 becomes critical to ensure

311   *S. pombe* cytokinesis and division during respiration due to decreased For3-dependent actin filament

312   nucleation elicited by SAPK activation.

313

314   ***Exogenous antioxidants bypass the need for Rlc1 phosphorylation to regulate myosin II activity and***

315   ***cytokinesis during respiratory growth***

316   In animal cells, aerobic respiration is accompanied by the production of reactive oxygen species

317   (ROS), which typically arise due to electron leakage from the mitochondrial electron transport chain [49].

318   *S. pombe* cells also produce free radicals during respiratory growth [50], and the ensuing endogenous

319   oxidative stress prompts Sty1 activation and an antioxidant response both at transcriptional and

320   translational levels [51] (Figure 6A). Remarkably, the increased Sty1 basal activity of wild-type and *rlc1-*

321   *S35A* cells growing with glycerol was largely counteracted in the presence of 0.16 mM of reduced

322   glutathione (GSH), an antioxidant tripeptide, and this was accompanied by a recover in total For3 levels

323   (Figure 6A). As expected, segmentation analysis confirmed that the cable-to-patch ratio was significantly

324   improved in glycerol-growing *rlc1-S35A* and *Myo2-E1* cells supplemented with GSH, compared to those

325   growing without the antioxidant (Figure 6B-C). Furthermore, the delayed CAR constriction and

326   disassembly, and the multiseptation of both *rlc1-S35A* or *Myo2-E1* cells during growth with glycerol,

327   were alleviated in the presence of GSH (Figure 6D-G). Most importantly, the simple addition of GSH

328   allowed *rlc1-S35A* and *Myo2-E1* cells to resume growth and proliferate in the presence of glycerol

329   (Figure 6H). This growth-recovery phenotype was For3-dependent since it was not shown by *rlc1-S35A*

330   *for3Δ* cells incubated in the presence of the antioxidant (Figure 6H). Hence, oxidative stress is the leading

331   cause of the formin-dependent reduction in the nucleation of actin cables, and imposes regulation of

332   Myo2 function by Rlc1 phosphorylation as a critical factor in the execution of cytokinesis during

333   respiration.

334

335

336   **Discussion**

337   RLC phosphorylation is a common regulatory mechanism of myosin II activity both in muscle

338   and non-muscle cells. RLC phosphorylation plays a key positive role as a regulator of myosin II function

339   in cardiac muscle contraction under normal and disease conditions [52]. Patients with heart failure usually

340   show reduced RLC phosphorylation, and restoring its normal phosphorylation status represents a

341   promising approach toward improving the function of the diseased heart [53]. In non-muscle vertebrate

342   cells, RLC phosphorylation at Ser19 is essential for NMII contractile activity during cell migration and

343   division [2, 7]. This also applies to invertebrates like *Drosophila melanogaster*, where *in vivo*

phosphorylation of *spaghetti-squash* RLC at the conserved Ser21 is critical to activate myosin II, thus

avoiding embryonic lethality and severe cytokinesis defects [54]. Contrariwise, in the unicellular amoeba

Dictyostelium discoideum RLC phosphorylation at the conserved Ser13 is not essential for regulating

Myosin II function, since expression of a non-phosphorylatable S13A mutant version fully rescues the

cytokinetic and developmental defects of RLC-null cells [55].

Despite also being a simple eukaryote, the effect of RLC phosphorylation on Myosin II activity

during cytokinesis in the fission yeast *S. pombe* has remained elusive. While some studies indicated that

lack of Rlc1 phosphorylation at the conserved Ser35 delays CAR constriction [17, 30], other works

suggest just the opposite [33]. This Crabtree-positive organism uses aerobic fermentation instead of

respiration for ATP production when glucose is available, whereas mitochondrial energy metabolism is

significantly reduced [56]. Importantly, and to our knowledge, the experimental setup in all the published

studies exploring the functional and mechanistic insights of fission yeast cytokinesis has relied on the

employment of wild-type and mutant cells growing fermentatively in glucose-rich minimal or complex

media. In these conditions, the impact of Rlc1 phosphorylation in cytokinesis is very modest since *rlc1-*

S35A cells show only a minimal delay in CAR constriction and disassembly compared to wild-type cells.

However, in this work, we show that this somehow secondary role becomes indispensable when yeast

cells switch to a respiratory metabolism in the absence of glucose. In this metabolic state, lack of Rlc1

phosphorylation at Ser35 resulted in a significant delay in the dynamics of CAR assembly and

disassembly, leading to a multiseptated phenotype and a decreased growth on respirable carbon sources

such as glycerol. Moreover, our findings also support that Myo2, the leading Myosin II heavy chain

isoform that regulates fission yeast CAR assembly and constriction under most conditions [57], is the

main regulatory target for Rlc1 Ser35 phosphorylation to allow *S. pombe* cytokinesis during respiration.

According to this view, the cytokinetic defects of cells expressing the hypomorphic allele *myo2-E1,*

which shows reduced ATPase activity and actin-filament binding [13], become notoriously exacerbated

during respiration and resemble those of *rlc1-S35A* cells. Therefore, the biological relevance of Rlc1

phosphorylation to modulate Myo2 activity *in vivo* for CAR assembly and constriction in *S. pombe*

strongly depends on the carbohydrate metabolism during the transition from fermentation to respiration.

Fission yeast p21-activated kinase Pak1 phosphorylates Rlc1 at Ser35 *in vivo* in glucose-rich

medium [30, 32]. However, genetic, biochemical, and cell biology evidences presented in this work

support that the second PAK ortholog Pak2 collaborates with Pak1 to phosphorylate Rlc1 at this residue

for adequate CAR contractility during respiratory growth (Figure 6—figure supplement 1). Accordingly,

thelack of activity of both kinases, but not each one separately, resulted in cytokinetic and respiratory

growth defects very similar to those shown by *rlc1-S35A* cells. Pak2 performs an important positive role

during the nitrogen starvation-induced sexual development in fission yeast, and Pak2-null cells show mating defects that result in the formation of aberrant asci [41]. We found that Pak2 levels, which are not detected during fermentative growth with glucose, are markedly induced upon nitrogen starvation and during respiratory growth in the absence of glucose through a transcriptional mechanism involving the Ste11 transcription factor. Importantly, Ste11 expression is in turn activated by Rst2, another transcription factor whose activity is strongly repressed in the presence of nitrogen and glucose by the cAMP-PKA pathway [43], thus restricting Pak2 availability and function to physiological contexts where either or both nutrients are not available. Hence, it seems very likely that in such scenarios Pak2 may target multiple protein substrates, some of them in a redundant fashion with Pak1, as a booster for PAK activity. Recent phosphoproteomic screens have identified additional Pak1 substrates besides Rlc1 that function in fermentative growth during cytokinesis, including the F-BAR protein Cdc15 or the anilin-like medial ring protein Mid1, and also during polarized growth, such as the Cdc42 GEF Scd1, the RhoGAP Rga4, or the cell end marker Tea3, among others [32]. However, the observation that Pak2 only localizes to the CAR during respiratory growth, suggests that its functional redundancy with Pak1 might be restricted to cytokinesis-associated proteins.

In animal cells, both de novo actin assembly at the division site and cortical transport/flow contribute with actin filaments for the CAR [58-60]. In fission yeast cells, which lack an actin filament cortex, the CAR is assembled chiefly by Myo2 from actin filaments nucleated *de novo* at the cytokinesis nodes by the essential formin Cdc12 and partially from Cdc12-nucleating actin cables pulled from non-equatorial region [61, 62]. However, further evidence demonstrated that actin filaments nucleated by For3, the formin that assembles the actin cables that participate in polarized secretion and growth, also contribute to CAR formation in fission yeast [24, 25]. In turn, the activated SAPK pathway down-regulates in *S. pombe* CAR assembly and stability in response to stress by reducing For3 levels [25, 63]. Like animal cells, fission yeast respiratory metabolism induces endogenous oxidative stress with electron leakage from the mitochondrial electron transport chain [49].This resulted in enhanced SAPK activation, downregulation of For3 levels, and a concomitant reduction in actin filaments. Our findings strongly support that in this metabolic situation, Rlc1 phosphorylation becomes critical regulating Myo2 function during cytokinesis due to a decrease in For3-nucleated actin filaments. Accordingly, recovery of actin filaments availability during respiration by alternative strategies, including the expression of a constitutively active For3 version, limitation of For3 downregulation in SAPK-less mutants, or attenuation of the endogenous metabolic oxidative stress with antioxidants (GSH), was sufficient to restore CAR assembly/constriction and cytokinesis both in *rlc1-S35A* and *myo2-E1* mutants during respiration, thus allowing cell growth. Compared to wild-type cells, the number of actin filaments at the

410 CAR is reduced approximately by half in *myo2-E1* cells [64], which might explain why enhanced

411 nucleation of actin filaments by For3 alleviates their defective actin-binding and motor activity during

412 cytokinesis.

413   Accumulating evidence suggests that metabolic reprogramming fuels the actin cytoskeletal

414 rearrangements that occur during the response of cells to external forces, epithelial-to-mesenchymal

415 transition, and cell migration. They are accompanied by glycolysis and oxidative phosphorylation

416 alterations that provide the required energy for these rearrangements [65-67]. However, a yet unanswered

417 question is how changes in cell metabolism prompt actin cytoskeletal remodeling [67]. Our observations

418 reveal a sophisticated adaptive interplay between modulation of Myosin II function by

419 Rlc1phosphorylation and environmentally controlled formin availability, which becomes critical for a

420 successful cytokinesis during a respiratory carbohydrate metabolism (Figure 6—figure supplement 1).

421 Altogether, these findings provide a remarkable example of how carbohydrate metabolism dictates the

422 relative importance of different sources of actin filaments for CAR dynamics during cellular division.

423

431

432 **Competing interests**

433 The authors declare that they have no conflict of interest.

434

435 **MATERIALS AND METHODS**

436 **Strain construction.**

437   *Schizosaccharomyces pombe* strains used in this work are listed in Supplementary Table S1.

438 Several deletion strains were obtained from the Bioneer mutant library [68], whereas null mutants in

439 *rlc1$^+$, pka1$^+$* and *ste11$^+$* genes were obtained by ORF deletion and replacement with G418 (kanR),

440 nourseothricin (NAT), or hygromycin B cassettes by employing a PCR-mediated strategy [69, 70], and

441 the oligonucleotides described in Supplementary Table S2. Strains expressing different genomic fusions

442 were constructed either by transformation or after random spore analysis of appropriate crosses in

443   sporulation agar (SPA) medium [71]. To generate a strain expressing an integrated Rlc1-HA fusion, the

444   *rlc1*[+] ORF plus its endogenous promoter were amplified by PCR using genomic DNA from *S. pombe*

445   972h[-] wild-type strain as the template and the 5' and 3´oligonucleotides PromRlc1(XhoI)-FWD and Rlc1-

446   GFP(SacII)-REV (Supplementary Table S2), which include, respectively, a *Xho*I restriction site and an

447   extended DNA sequence encoding a HA C-terminal tag plus a *Sac*II site. The *Xho*I-*Sac*II digested PCR

448   fragment was cloned into plasmid pJK210 [72], sequenced, linearized with *Bmg*BI, and transformed into

449   an *rlc1Δ ura4.294* strain. To obtain a strain expressing an integrative Rlc1-HA fusion under the control of

450   the β-estradiol promoter [37], the *rlc1*[+] ORF fused to a 3´ HA tag was amplified by PCR 5' and

451   3´oligonucleotides Rlc1 (SmaI)- FWD and Rlc1-HA (SacII)-REV, which include, respectively, *Sma*I and

452   *Sac*II restriction sites. The amplified PCR product was cloned into a modified plasmid pJK210 containing

453   a β-estradiol regulated promoter Z$_3$EV [37], and the resulting construct was linearized with *Stu*I, and

454   transformed into an *rlc1Δ ura4.294* strain. To obtain a strain expressing an integrative Rlc1-GFP fusion,

455   DNA encoding an Rlc1-GFP fusion under the endogenous promoter was amplified by PCR using as the

456   template a genomic DNA from a *S. pombe* strain expressing a genomic Rlc1-GFP fusion (Supplementary

457   Table S1), and the 5' and 3´oligonucleotides PromRlc1(XhoI)-FWD and Rlc1-GFP(SacII)-REV, which

458   include *Sma*I and *Sac*II restriction sites, respectively. The resulting DNA fragment was cloned into

459   plasmid pJK210, linearized with *Stu*I, and transformed into an *rlc1Δ ura4.294* strain. In all cases Ura4^{+}

460   transformants were obtained, and the correct integration and expression of the Rlc1-HA and Rlc1-GFP

461   fusions fusion under either the endogenous or the β-estradiol regulated promoters were verified by both

462   PCR and Western blot analysis, respectively. To generate strains expressing Rlc1-HA and Rlc1-GFP

463   versions with mutations at Ser35 and/or Ser36 residues to Alanine, the pJK210 plasmids described above

464   containing either Rlc1-GFP or Rlc1-HA fusions were subjected as templates to site-directed mutagenesis

465   by PCR, by employing specific mutagenic oligonucleotides described in Supplementary Table S2. Then

466   mutagenized plasmids were linearized with *Bmg*BI and transformed into an *rlc1Δ ura4.294* strain.

467   The *S. pombe* strain expressing a genomic Pak2-3GFP fusion was obtained in two successive

468   steps. First, the *pak2*[+] ORF plus its endogenous promoter were amplified by PCR using genomic DNA

469   from *S. pombe* 972h[-] wild-type strain as the template, and the 5' and 3´oligonucleotides PromPak2(XhoI)-

470   FWD (*Xho*I site) and Pak2GFP(SmaI/XmaI)-REV (*Sma*I site) (Supplementary Table S2). The PCR

471   product was cloned in frame into a pJK210 plasmid containing a GFP C-terminal Tag. In a second step,

472   this construct was linearized with *Sma*I and two additional GFP tags were added by a Gibson assembly

473   approach. Finally, the resulting plasmid was linearized with *Bmg*BI and transformed in a *pak2Δ ura4.294*

474   strain. To introduce the mutations at the two putative Ste11-binding motifs in Pak2 promoter (TR box),

475   the pJK210-Pak2-3GFP plasmid was subjected to sequential site-directed mutagenesis by PCR. In this

476   way, the conserved G in each motif was replaced by A by employing the mutagenic oligonucleotides

477   described in Supplementary Table S2. To generate a strain producing a Pak2-GFP fusion under the

478   control of Pak1 promoter, Pak1 5´UTR sequence was amplified by PCR using genomic DNA from *S.*

479   *pombe* 972h⁻ wild-type strain and assembled by Gibson cloning to a PCR-amplified Pak2-GFP fragment

480   and the pJK210 plasmid linearized with *Sma*I. The resulting plasmid was digested with *Bmg*BI and

481   transformed in a *pak2Δ ura4.294* strain.

482

483   **Media and growth conditions.**

484   In experiments performed with liquid cultures, fission yeast strains were grown overnight with

485   shaking at 28°C in YES-Glucose medium, which includes 0.6% yeast extract, 2% glucose, and is

486   supplemented with adenine, leucine, histidine, or uracil (100 mg/liter) [73]. The next day, cultures were

487   diluted to an OD_{600} of 0.01 and incubated until reaching a final OD_{600} of 0.2. Then, cells were recovered

488   by filtration, washed three times, and shifted to either YES-Glucose or YES-Glycerol (0.6% yeast extract,

489   0.08% glucose, 0.86% glycerol, plus supplements), and incubated at 28ºC for 4 h before imaging. In

490   experiments performed with the *Myo2-E1* mutant, cells recovered from cultures at 28ºC were resuspended

491   in YES-Glucose or YES-Glycerol, incubated at 30ºC for 2 h, and then at 28ºC for the remainder of the

492   experiment. In experiments with cells expressing the analogue-sensitive Cdc2 (CDK) kinase version

493   *cdc2-asM17* [35], cells from log-phase liquid cultures in YES-Glucose (OD_{600} 0.5), were treated with 1

494   µM 3-NM-PP1 (Sigma-Aldrich, 529581) for 3.5 h, recovered by filtration, washed, and resuspended in

495   YES-Glucose medium. In experiments with strains expressing an analog-sensitive Pak1 kinase version

496   Pak1-M460A, log-phase liquid cultures were divided in two and incubated for different times in YES-

497   Glucose medium treated with 10 µM 3-BrB-PP1 (Abcam, ab143756), or in medium lacking the analog

498   kinase inhibitor. In nitrogen starvation experiments, strains growing exponentially in Edinburgh Minimal

499   Medium (EMM2)[74] with 2% glucose (OD_{600} 0.5), were recovered by filtration and resuspended in the

500   same medium lacking ammonium chloride for the indicated times. In the plate assays of stress sensitivity

501   for growth, *S. pombe* wild-type and mutant strains were grown in YES-Glucose liquid medium to an

502   OD_{600} of 1.2, recovered by centrifugation, resuspended in YES to a density of 10^7 cells/ml, and

503   appropriate decimal dilutions were spotted on YES-Glucose (2% glucose), or YES-Glycerol (0.08%

504   glucose plus 3% glycerol), solid plates (2% agar). Plates were incubated for 3 days (YES-Glucose), or 5

505   days (YES-Glycerol), at different temperatures (28ºC, 30ºC, 32ºC, and/or 34ºC), depending on the

506   experiment, and then photographed. All the assays were repeated at least three times with similar results.

507   Representative experiments are shown in the corresponding Figures. When required, solid and or liquid

508 media were supplemented with varying amounts of β-estradiol (Sigma-Aldrich, RPN2106), or reduced

509 glutathione (GSH; Sigma-Aldrich, G6013).

510

511 **Microscopy analysis.**

512 For *time-lapse* imaging of CAR dynamics, 300 µl of cells growing exponentially for 4 h in YES-

513 Glucose or YES-Glycerol liquid medium, and prepared as described above, were placed in a well from a

514 µ-Slide eight well (Ibidi, 80826), previously coated with 10 µl of 1 mg/ml soybean lectin (Sigma-Aldrich,

515 L2650) [25]. When required, GSH was incorporated into the medium at a final concentration of 0.3 mM.

516 Cells were left to sediment in the culture media and attach to the well bottom for 1 min, and images were

517 captured every 2.5 min for 2 h in YES-Glucose cultures, or every 5 min for 8 h in YES-Glycerol cultures.

518 Experiments were performed at 28°C, and single middle planes from a set of six stacks (0.61 µm each)

519 were taken at the indicated time points. Time-lapse images were acquired using a Leica Stellaris 8

520 confocal microscope with a 63X/1.40 Plan Apo objective and controlled by the LAS X software. The time

521 for node condensation and ring maturation includes the time from SPB separation until the start of CR

522 constriction. The time for ring constriction and disassembly includes the time from the first frame of ring

523 constriction until the last frame where it becomes completely constricted and disassembled. The total time

524 for ring assembly and disassembly is the sum of these two values. *n* is the total number of cells scored

525 from at least three independent experiments. Statistical comparison between two groups was performed

526 by unpaired Student's *t-test.*

527 To perform actin staining with Alexa-Fluor phalloidin, 5 ml mid-log cultures in YES-Glucose

528 (OD_{600} 0.5), or YES-Glycerol (OD_{600} 0.2), were grown for 12 h after media shift. Cells were fixed by

529 shacking for 1 h with 3.7% formaldehyde in PEM buffer (10 mM EGTA; 1 mM $MgSO_4$; 100 mM PIPES

530 pH 6.9, 75 mM sucrose and 0.1% Triton X-100). After three washes with PEM, the cell pellets were

531 resuspended in 20 µl of cold 40% methanol solution, stained with 8 µl of 5 mg/ml Alexa fluor 488-

532 conjugated phalloidin (Thermo Fisher Scientific, A12379), and incubated in a rotary platform overnight at

533 4ºC in the dark. Images of stained cells were acquired from samples spotted on glass slides with a Leica

534 Stellaris 8 confocal microscope using a 100X/1.40 Plan Apo objective (7 stacks of 0.3 µm each). For

535 actin segmentation analysis, the Ilastik routine with the Pixel classification tool [45], was trained with two

536 representative images, one from cell growing in YES-Glucose medium, and one with cells growing in

537 YES-Glycerol. The training involves drawing cables, patches and background in three different colors.

538 Once the program was trained, the remaining images from the different experiments were uploaded to

539 Ilastik to perform the segmentation routine. The resulting images were then exported to ImageJ [75], and

540 segmented cells at G2 were analysed using the color histogram tool, obtaining the specific areas

541   corresponding to cables and patches. The data from n ≥ 40 cells growing in YES-Glycerol were obtained

542   for each cell by dividing the cable area by the patch area, and the ratio was normalized with respect to the

543   average obtained from wild-type cells growing with YES-Glucose medium. To perform For3-GFP

544   quantification Ilastik was trained drawing For3-GFP dots, GFP background and image background in

545   three different colors. The For3-GFP patch to cytosol ratio was calculated by dividing the For3-GFP color

546   area between the GFP background area from at least n ≥ 40 cells in G2 or late M (dividing cells) and

547   normalized with the average of the glucose ratio.

548   For cell wall staining, fission yeast cells were cultured in YES-Glucose or YES-Glycerol for

549   different times in the absence or presence of 0.3 mM of GSH. Cells from 1 ml aliquots were recovered by

550   centrifugation, stained with 1 µl of 0.5 mg/ml calcofluor white, and images were acquired from samples

551   spotted on glass slides with a Leica Stellaris 8 confocal microscope using a 63X/1.40 Plan Apo objective

552   (6 stacks of 0.61 µm each). The percentage of septated (one septa), multiseptated (two or more septa), and

553   lysed cells, was calculated at the indicated time points for each strain and condition from three

554   independent experiments. n≥ 100 cells were counted from several images captured during each replicate.

555

556   **Western blot analysis.**

557   To detect levels of Rlc1-HA fusion and/or its phosphorylation status, fission yeast cultures were

558   grown in YES-Glucose or YES-Glycerol as described above, and 10 ml samples were collected and

559   precipitated with TCA [76]. Protein extracts were resolved in 15% SDS-PAGE gels, transferred to

560   nitrocellulose blotting membranes, and immunoblotted with a mouse monoclonal anti-HA antibody

561   (clone 12CA5; Roche, 11 583 816 001, RRID:AB_514505). Rabbit monoclonal anti-PSTAIR (anti-Cdc2;

562   Sigma-Aldrich, 06-923, RRID:AB_310302) was used for loading control. Immunoreactive bands were

563   revealed, respectively, with anti-mouse (Abcam, ab205719, RRID:AB_2755049), and anti-rabbit HRP-

564   conjugated secondary antibodies (Abcam, ab205718, RRID:AB_2819160), and the ECL system (GE-

565   Healthcare, RPN2106). For detection of Pak1-GFP and Pak2-3GFP fusions, the TCA-precipitated protein

566   extracts were resolved in 6% SDS-PAGE gels, transferred to nitrocellulose membranes, and incubated

567   with a mouse monoclonal anti-GFP antibody (Roche, 11 814 460 001, RRID:AB_390913), and anti-cdc2

568   (PSTAIR), as a loading control. To determine For3-3GFP and For3(DAD)-2GFP levels, total protein

569   extracts from exponentially growing cultures were obtained under native conditions with lysis buffer (20

570   mM Tris-HCl pH 8.0, 2 mM EDTA, 100 mM NaCl, and 0.5% NP-40, plus a protease inhibitor cocktail).

571   Proteins were resolved in 6% SDS-PAGE gels and transferred to Hybond-ECL membranes. For3-GFP

572   fusions were detected with a mouse monoclonal anti-GFP antibody (Roche), with anti-cdc2 (PSTAIR) as

573   a loading control. In all cases the immunoreactive bands were revealed with anti-mouse or anti-rabbit

574   HRP-conjugated secondary antibodies and the ECL system.

575   To detect Sty1 phosphorylation and total protein levels in strains expressing a genomic Sty1-HA

576   fusion, cell samples of 5 ml were collected at the indicated times and immediately centrifuged for 20 s at

577   3200 rpm/4ºC. The cell pellets were resuspended in 1 ml of ice-cold buffer (10 mM $NaPO_4$, 0.5 mM

578   EDTA pH 7.5), transferred to 1.5 ml tubes, centrifuged at 13000 rpm/4˚C, and stored at 80ºC until further

579   processing. Cell lysis was achieved in a FastPrep instrument after mixing the cell pellets with pre-chilled

580   0.5 mm glass beads to −20ºC with ice-cold lysis buffer (20 mM Tris-HCl pH 8.0, 2 mM EDTA, 100 mM

581   NaCl, and 0.5% NP-40 and containing a protease inhibitor cocktail) (Sigma Aldrich, P8340). The cell

582   lysates were clarified by centrifugation at 13000 rpm/4°C for 5 min, and the protein extracts were

583   resolved in 12% SDS-PAGE gels and transferred to nitrocellulose membranes. Dual phosphorylation of

584   Sty1 was detected employing a rabbit polyclonal anti-phospho-p38 antibody (Cell Signaling, 9211,

585   RRID:AB_331641). Total Sty1 was detected in *S. pombe* extracts with mouse monoclonal anti-HA

586   antibody (12CA5, Roche). Immunoreactive bands were revealed with anti-mouse or anti-rabbit HRP-

587   conjugated secondary antibodies (Abcam), and the ECL system.

588   Densitometric quantification of Western blot experiments as of 16-bit. jpg digital images of blots

589   was performed using ImageJ [75]. The desired bands plus background were drawn as rectangles and a

590   profile plot (peak) was obtained for each band. To reduce the background noise in the bands, each peak

591   floating above the baseline of the corresponding peak was manually closed off using the straight-line tool.

592   Measurement of the closed peaks was performed with the wand tool. Relative Units (R.U.) of For3 levels

593   were estimated by determining the signal ratio of the correspondent anti-GFP (total For3) blot with

594   respect to the anti-cdc2 blot (internal control) at each time point. Quantification data correspond to

595   experiments performed as biological triplicates. Mean relative units ± SD are shown.

596

597   **Statistical analysis.**

598   Statistical analysis was performed using prism 6 software (Graph pad), and results are represented

599   as mean ± SD, unless otherwise indicated. Comparisons for two groups were calculated using unpaired

600   two-tailed Student's t-tests, whereas comparisons of more than two groups were calculated using one-way

601   ANOVA with Bonferroni's multiple comparison tests. We observed normal distribution and no difference

602   in variance between groups in individual comparisons. Statistical significance: * $p<0.05$; ** $p < 0.005$;

603   *** $p < 0.0005$; **** $p < 0.0001$. Further details on statistical analysis are included in the figure legends.

604

605   **Data availability**

606   All data generated or analyzed during this study are included in the manuscript and supporting files.

607

References

609   1.   Green RA, Paluch E, Oegema K. Cytokinesis in animal cells. Annu Rev Cell Dev Biol. 2012;28:29-
610   58. Epub 20120709. doi: 10.1146/annurev-cellbio-101011-155718. PubMed PMID: 22804577.

611   2.   Garrido-Casado M, Asensio-Juárez G, Vicente-Manzanares M. Nonmuscle Myosin II Regulation
612   Directs Its Multiple Roles in Cell Migration and Division. Annu Rev Cell Dev Biol. 2021;37:285-310. Epub
613   20210727. doi: 10.1146/annurev-cellbio-042721-105528. PubMed PMID: 34314591.

614   3.   Mangione MC, Gould KL. Molecular form and function of the cytokinetic ring. J Cell Sci.
615   2019;132(12). Epub 2019/06/19. doi: 10.1242/jcs.226928. PubMed PMID: 31209062; PubMed Central
616   PMCID: PMCPMC6602304.

617   4.   Craig R, Smith R, Kendrick-Jones J. Light-chain phosphorylation controls the conformation of
618   vertebrate non-muscle and smooth muscle myosin molecules. Nature. 1983;302(5907):436-9. doi:
619   10.1038/302436a0. PubMed PMID: 6687627.

620   5.   Trybus KM, Lowey S. Conformational states of smooth muscle myosin. Effects of light chain
621   phosphorylation and ionic strength. J Biol Chem. 1984;259(13):8564-71. PubMed PMID: 6610679.

622   6.   Trybus KM. Filamentous smooth muscle myosin is regulated by phosphorylation. J Cell Biol.
623   1989;109(6 Pt 1):2887-94. doi: 10.1083/jcb.109.6.2887. PubMed PMID: 2531749; PubMed Central
624   PMCID: PMCPMC2115938.

625   7.   Komatsu S, Yano T, Shibata M, Tuft RA, Ikebe M. Effects of the regulatory light chain
626   phosphorylation of myosin II on mitosis and cytokinesis of mammalian cells. J Biol Chem.
627   2000;275(44):34512-20. doi: 10.1074/jbc.M003019200. PubMed PMID: 10944522.

628   8.   Bao J, Jana SS, Adelstein RS. Vertebrate nonmuscle myosin II isoforms rescue small interfering
629   RNA-induced defects in COS-7 cell cytokinesis. J Biol Chem. 2005;280(20):19594-9. Epub 20050317. doi:
630   10.1074/jbc.M501573200. PubMed PMID: 15774463.

631   9.   Ma X, Jana SS, Conti MA, Kawamoto S, Claycomb WC, Adelstein RS. Ablation of nonmuscle
632   myosin II-B and II-C reveals a role for nonmuscle myosin II in cardiac myocyte karyokinesis. Mol Biol Cell.
633   2010;21(22):3952-62. Epub 20100922. doi: 10.1091/mbc.E10-04-0293. PubMed PMID: 20861308;
634   PubMed Central PMCID: PMCPMC2982113.

635   10.   Pollard TD, Wu JQ. Understanding cytokinesis: lessons from fission yeast. Nat Rev Mol Cell Biol.
636   11. England2010. p. 149-55.

637   11.   Rincon SA, Paoletti A. Molecular control of fission yeast cytokinesis. Semin Cell Dev Biol.
638   2016;53:28-38. Epub 2016/01/26. doi: 10.1016/j.semcdb.2016.01.007. PubMed PMID: 26806637.

639   12.   Balasubramanian MK, Bi E, Glotzer M. Comparative analysis of cytokinesis in budding yeast,
640   fission yeast and animal cells. Curr Biol. 2004;14(18):R806-18. Epub 2004/09/24. doi:
641   10.1016/j.cub.2004.09.022. PubMed PMID: 15380095.

642   13.   Wang K, Okada H, Bi E. Comparative Analysis of the Roles of Non-muscle Myosin-IIs in
643   Cytokinesis in Budding Yeast, Fission Yeast, and Mammalian Cells. Front Cell Dev Biol. 2020;8:593400.
644   Epub 20201119. doi: 10.3389/fcell.2020.593400. PubMed PMID: 33330476; PubMed Central PMCID:
645   PMCPMC7710916.

646   14.   Laplante C, Berro J, Karatekin E, Hernandez-Leyva A, Lee R, Pollard TD. Three myosins contribute
647   uniquely to the assembly and constriction of the fission yeast cytokinetic contractile ring. Curr Biol.
648   2015;25(15):1955-65. Epub 20150702. doi: 10.1016/j.cub.2015.06.018. PubMed PMID: 26144970;
649   PubMed Central PMCID: PMCPMC4526439.

650   15.   Palani S, Chew TG, Ramanujam S, Kamnev A, Harne S, Chapa YLB, et al. Motor Activity
651   Dependent and Independent Functions of Myosin II Contribute to Actomyosin Ring Assembly and
652   Contraction in Schizosaccharomyces pombe. Curr Biol. 2017;27(5):751-7. Epub 20170223. doi:
653   10.1016/j.cub.2017.01.028. PubMed PMID: 28238661; PubMed Central PMCID: PMCPMC5344676.

654   16.   Okada H, Wloka C, Wu JQ, Bi E. Distinct Roles of Myosin-II Isoforms in Cytokinesis under Normal
655   and Stressed Conditions. iScience. 2019;14:69-87. Epub 2019/04/01. doi: 10.1016/j.isci.2019.03.014.
656   PubMed PMID: 30928696; PubMed Central PMCID: PMCPMC6441717.

657   17.   Pollard LW, Bookwalter CS, Tang Q, Krementsova EB, Trybus KM, Lowey S. Fission yeast myosin
658   Myo2 is down-regulated in actin affinity by light chain phosphorylation. Proc Natl Acad Sci U S A.
659   2017;114(35):E7236-e44. Epub 2017/08/16. doi: 10.1073/pnas.1703161114. PubMed PMID: 28808035;
660   PubMed Central PMCID: PMCPMC5584420.

661   18.   Laporte D, Coffman VC, Lee IJ, Wu JQ. Assembly and architecture of precursor nodes during
662   fission yeast cytokinesis. J Cell Biol. 2011;192(6):1005-21. doi: 10.1083/jcb.201008171. PubMed PMID:
663   21422229; PubMed Central PMCID: PMCPMC3063137.

664   19.   McDonald NA, Lind AL, Smith SE, Li R, Gould KL. Nanoscale architecture of the
665   Schizosaccharomyces pombe contractile ring. Elife. 2017;6. Epub 2017/09/16. doi: 10.7554/eLife.28865.
666   PubMed PMID: 28914606; PubMed Central PMCID: PMCPMC5779233.

667   20.   Laplante C, Huang F, Tebbs IR, Bewersdorf J, Pollard TD. Molecular organization of cytokinesis
668   nodes and contractile rings by super-resolution fluorescence microscopy of live fission yeast. Proc Natl
669   Acad Sci U S A. 2016;113(40):E5876-e85. Epub 20160919. doi: 10.1073/pnas.1608252113. PubMed
670   PMID: 27647921; PubMed Central PMCID: PMCPMC5056082.

671   21.   Chang F, Drubin D, Nurse P. cdc12p, a protein required for cytokinesis in fission yeast, is a
672   component of the cell division ring and interacts with profilin. J Cell Biol. 1997;137(1):169-82. Epub
673   1997/04/07. doi: 10.1083/jcb.137.1.169. PubMed PMID: 9105045; PubMed Central PMCID:
674   PMCPMC2139860.

675   22.   Kovar DR, Kuhn JR, Tichy AL, Pollard TD. The fission yeast cytokinesis formin Cdc12p is a barbed
676   end actin filament capping protein gated by profilin. J Cell Biol. 2003;161(5):875-87. Epub 2003/06/11.
677   doi: 10.1083/jcb.200211078. PubMed PMID: 12796476; PubMed Central PMCID: PMCPMC2172974.

678   23.   Vavylonis D, Wu JQ, Hao S, O'Shaughnessy B, Pollard TD. Assembly mechanism of the contractile
679   ring for cytokinesis by fission yeast. Science. 2008;319(5859):97-100. Epub 20071213. doi:
680   10.1126/science.1151086. PubMed PMID: 18079366.

681   24.   Coffman VC, Sees JA, Kovar DR, Wu JQ. The formins Cdc12 and For3 cooperate during contractile
682   ring assembly in cytokinesis. J Cell Biol. 2013;203(1):101-14. Epub 2013/10/16. doi:
683   10.1083/jcb.201305022. PubMed PMID: 24127216; PubMed Central PMCID: PMCPMC3798249.

684   25.   Gómez-Gil E, Martín-García R, Vicente-Soler J, Franco A, Vázquez-Marín B, Prieto-Ruiz F, et al.
685   Stress-activated MAPK signalling controls fission yeast actomyosin ring integrity by modulating formin
686   For3 levels. Elife. 2020;9. Epub 2020/09/12. doi: 10.7554/eLife.57951. PubMed PMID: 32915139.

687   26.   Willet AH, McDonald NA, Gould KL. Regulation of contractile ring formation and septation in
688   Schizosaccharomyces pombe. Curr Opin Microbiol. 2015;28:46-52. Epub 2015/09/05. doi:
689   10.1016/j.mib.2015.08.001. PubMed PMID: 26340438; PubMed Central PMCID: PMCPMC4688203.

690   27.   Le Goff X, Motegi F, Salimova E, Mabuchi I, Simanis V. The S. pombe rlc1 gene encodes a
691   putative myosin regulatory light chain that binds the type II myosins myo3p and myo2p. J Cell Sci.
692   2000;113 Pt 23:4157-63. PubMed PMID: 11069761.

693   28.   Naqvi NI, Wong KC, Tang X, Balasubramanian MK. Type II myosin regulatory light chain relieves
694   auto-inhibition of myosin-heavy-chain function. Nat Cell Biol. 2000;2(11):855-8. doi: 10.1038/35041107.
695   PubMed PMID: 11056543.

696   29.   McCollum D, Balasubramanian MK, Pelcher LE, Hemmingsen SM, Gould KL.
697   Schizosaccharomyces pombe cdc4+ gene encodes a novel EF-hand protein essential for cytokinesis. J
698   Cell Biol. 1995;130(3):651-60. doi: 10.1083/jcb.130.3.651. PubMed PMID: 7622565; PubMed Central
699   PMCID: PMCPMC2120525.

700   30.   Loo TH, Balasubramanian M. Schizosaccharomyces pombe Pak-related protein, Pak1p/Orb2p,
701   phosphorylates myosin regulatory light chain to inhibit cytokinesis. J Cell Biol. 2008;183(5):785-93. Epub
702   20081124. doi: 10.1083/jcb.200806127. PubMed PMID: 19029336; PubMed Central PMCID:
703   PMCPMC2592837.

704   31.   Chew TL, Masaracchia RA, Goeckeler ZM, Wysolmerski RB. Phosphorylation of non-muscle
705   myosin II regulatory light chain by p21-activated kinase (gamma-PAK). J Muscle Res Cell Motil.
706   1998;19(8):839-54. doi: 10.1023/a:1005417926585. PubMed PMID: 10047984.

707   32.   Magliozzi JO, Sears J, Cressey L, Brady M, Opalko HE, Kettenbach AN, et al. Fission yeast Pak1
708   phosphorylates anillin-like Mid1 for spatial control of cytokinesis. J Cell Biol. 2020;219(8). Epub
709   2020/05/19. doi: 10.1083/jcb.201908017. PubMed PMID: 32421151; PubMed Central PMCID:
710   PMCPMC7401808.

711   33.   Sladewski TE, Previs MJ, Lord M. Regulation of fission yeast myosin-II function and contractile
712   ring dynamics by regulatory light-chain and heavy-chain phosphorylation. Mol Biol Cell.
713   2009;20(17):3941-52. Epub 20090701. doi: 10.1091/mbc.e09-04-0346. PubMed PMID: 19570908;
714   PubMed Central PMCID: PMCPMC2735492.

715   34.   Stark BC, Sladewski TE, Pollard LW, Lord M. Tropomyosin and myosin-II cellular levels promote
716   actomyosin ring assembly in fission yeast. Mol Biol Cell. 2010;21(6):989-1000. Epub 20100128. doi:
717   10.1091/mbc.e09-10-0852. PubMed PMID: 20110347; PubMed Central PMCID: PMCPMC2836979.

718   35.   Aoi Y, Kawashima SA, Simanis V, Yamamoto M, Sato M. Optimization of the analogue-sensitive
719   Cdc2/Cdk1 mutant by in vivo selection eliminates physiological limitations to its use in cell cycle analysis.

720   Open Biol. 2014;4(7). Epub 2014/07/06. doi: 10.1098/rsob.140063. PubMed PMID: 24990387; PubMed
721   Central PMCID: PMCPMC4118601.

722   36.   Malecki M, Bitton DA, Rodríguez-López M, Rallis C, Calavia NG, Smith GC, et al. Functional and
723   regulatory profiling of energy metabolism in fission yeast. Genome Biol. 2016;17(1):240. Epub
724   20161125. doi: 10.1186/s13059-016-1101-2. PubMed PMID: 27887640; PubMed Central PMCID:
725   PMCPMC5124322.

726   37.   Ohira MJ, Hendrickson DG, Scott McIsaac R, Rhind N. An estradiol-inducible promoter enables
727   fast, graduated control of gene expression in fission yeast. Yeast. 2017;34(8):323-34. Epub 2017/04/20.
728   doi: 10.1002/yea.3235. PubMed PMID: 28423198; PubMed Central PMCID: PMCPMC5542879.

729   38.   Sells MA, Barratt JT, Caviston J, Ottilie S, Leberer E, Chernoff J. Characterization of Pak2p, a
730   pleckstrin homology domain-containing, p21-activated protein kinase from fission yeast. J Biol Chem.
731   1998;273(29):18490-8. doi: 10.1074/jbc.273.29.18490. PubMed PMID: 9660818.

732   39.   Yang P, Kansra S, Pimental RA, Gilbreth M, Marcus S. Cloning and characterization of shk2, a
733   gene encoding a novel p21-activated protein kinase from fission yeast. J Biol Chem. 1998;273(29):18481-
734   9. doi: 10.1074/jbc.273.29.18481. PubMed PMID: 9660817.

735   40.   Mata J, Bähler J. Global roles of Ste11p, cell type, and pheromone in the control of gene
736   expression during early sexual differentiation in fission yeast. Proc Natl Acad Sci U S A.
737   2006;103(42):15517-22. Epub 20061009. doi: 10.1073/pnas.0603403103. PubMed PMID: 17032641;
738   PubMed Central PMCID: PMCPMC1592531.

739   41.   Vještica A, Merlini L, Nkosi PJ, Martin SG. Gamete fusion triggers bipartite transcription factor
740   assembly to block re-fertilization. Nature. 2018;560(7718):397-400. Epub 20180808. doi:
741   10.1038/s41586-018-0407-5. PubMed PMID: 30089908.

742   42.   Sugimoto A, Iino Y, Maeda T, Watanabe Y, Yamamoto M. Schizosaccharomyces pombe ste11+
743   encodes a transcription factor with an HMG motif that is a critical regulator of sexual development.
744   Genes Dev. 1991;5(11):1990-9. doi: 10.1101/gad.5.11.1990. PubMed PMID: 1657709.

745   43.   Kunitomo H, Higuchi T, Iino Y, Yamamoto M. A zinc-finger protein, Rst2p, regulates transcription
746   of the fission yeast ste11(+) gene, which encodes a pivotal transcription factor for sexual development.
747   Mol Biol Cell. 2000;11(9):3205-17. Epub 2000/09/12. doi: 10.1091/mbc.11.9.3205. PubMed PMID:
748   10982411; PubMed Central PMCID: PMCPMC14986.

749   44.   Madrid M, Soto T, Franco A, Paredes V, Vicente J, Hidalgo E, et al. A cooperative role for Atf1
750   and Pap1 in the detoxification of the oxidative stress induced by glucose deprivation in
751   Schizosaccharomyces pombe. Journal of Biological Chemistry. 2004;279(40):41594-602. doi:
752   10.1074/jbc.M405509200. PubMed PMID: WOS:000224075500044.

753   45.   Berg S, Kutra D, Kroeger T, Straehle CN, Kausler BX, Haubold C, et al. ilastik: interactive machine
754   learning for (bio)image analysis. Nat Methods. 2019;16(12):1226-32. Epub 20190930. doi:
755   10.1038/s41592-019-0582-9. PubMed PMID: 31570887.

756   46.   Martin SG, Rincon SA, Basu R, Perez P, Chang F. Regulation of the formin for3p by cdc42p and
757   bud6p. Mol Biol Cell. 2007;18(10):4155-67. Epub 2007/08/19. doi: 10.1091/mbc.e07-02-0094. PubMed
758   PMID: 17699595; PubMed Central PMCID: PMCPMC1995706.

759   47.   Perez P, Cansado J. Cell Integrity Signaling and Response to Stress in Fission Yeast. Current
760   Protein & Peptide Science. 2010;11(8):680-92. doi: 10.2174/138920310794557718. PubMed PMID:
761   WOS:000287357000005.

762   48.   Alonso-Matilla R, Thiyagarajan S, O'Shaughnessy B. Sliding filament and fixed filament
763   mechanisms contribute to ring tension in the cytokinetic contractile ring. Cytoskeleton (Hoboken).
764   2019;76(11-12):611-25. Epub 2019/08/24. doi: 10.1002/cm.21558. PubMed PMID: 31443136.

765   49.   Farrugia G, Balzan R. Oxidative stress and programmed cell death in yeast. Front Oncol.
766   2012;2:64. Epub 20120620. doi: 10.3389/fonc.2012.00064. PubMed PMID: 22737670; PubMed Central
767   PMCID: PMCPMC3380282.

768   50.   Zuin A, Gabrielli N, Calvo IA, García-Santamarina S, Hoe KL, Kim DU, et al. Mitochondrial
769   dysfunction increases oxidative stress and decreases chronological life span in fission yeast. PLoS One.
770   2008;3(7):e2842. Epub 2008/07/31. doi: 10.1371/journal.pone.0002842. PubMed PMID: 18665268;
771   PubMed Central PMCID: PMCPMC2475502.

772   51.   Zuin A, Castellano-Esteve D, Ayté J, Hidalgo E. Living on the edge: stress and activation of stress
773   responses promote lifespan extension. Aging (Albany NY). 2010;2(4):231-7. doi: 10.18632/aging.100133.
774   PubMed PMID: 20453258; PubMed Central PMCID: PMCPMC2881511.

775   52.   Yuan CC, Muthu P, Kazmierczak K, Liang J, Huang W, Irving TC, et al. Constitutive
776   phosphorylation of cardiac myosin regulatory light chain prevents development of hypertrophic
777   cardiomyopathy in mice. Proc Natl Acad Sci U S A. 2015;112(30):E4138-46. Epub 20150629. doi:
778   10.1073/pnas.1505819112. PubMed PMID: 26124132; PubMed Central PMCID: PMCPMC4522794.

779   53.   Markandran K, Poh JW, Ferenczi MA, Cheung C. Regulatory Light Chains in Cardiac Development
780   and Disease. Int J Mol Sci. 2021;22(9). Epub 20210421. doi: 10.3390/ijms22094351. PubMed PMID:
781   33919432; PubMed Central PMCID: PMCPMC8122660.

782   54.   Jordan P, Karess R. Myosin light chain-activating phosphorylation sites are required for
783   oogenesis in Drosophila. J Cell Biol. 1997;139(7):1805-19. doi: 10.1083/jcb.139.7.1805. PubMed PMID:
784   9412474; PubMed Central PMCID: PMCPMC2132636.

785   55.   Ostrow BD, Chen P, Chisholm RL. Expression of a myosin regulatory light chain phosphorylation
786   site mutant complements the cytokinesis and developmental defects of Dictyostelium RMLC null cells. J
787   Cell Biol. 1994;127(6 Pt 2):1945-55. doi: 10.1083/jcb.127.6.1945. PubMed PMID: 7806572; PubMed
788   Central PMCID: PMCPMC2120314.

789   56.   Malina C, Yu R, Björkeroth J, Kerkhoven EJ, Nielsen J. Adaptations in metabolism and protein
790   translation give rise to the Crabtree effect in yeast. Proc Natl Acad Sci U S A. 2021;118(51). Epub
791   2021/12/15. doi: 10.1073/pnas.2112836118. PubMed PMID: 34903663.

792   57.   Zambon P, Palani S, Kamnev A, Balasubramanian MK. Myo2p is the major motor involved in
793   actomyosin ring contraction in fission yeast. Curr Biol. 2017;27(3):R99-r100. doi:
794   10.1016/j.cub.2016.12.024. PubMed PMID: 28171765; PubMed Central PMCID: PMCPMC5300900.

795   58.   Cao LG, Wang YL. Mechanism of the formation of contractile ring in dividing cultured animal
796   cells. I. Recruitment of preexisting actin filaments into the cleavage furrow. J Cell Biol. 1990;110(4):1089-
797   95. doi: 10.1083/jcb.110.4.1089. PubMed PMID: 2324193; PubMed Central PMCID: PMCPMC2116085.

798   59.   Khaliullin RN, Green RA, Shi LZ, Gomez-Cavazos JS, Berns MW, Desai A, et al. A positive-
799   feedback-based mechanism for constriction rate acceleration during cytokinesis in Caenorhabditis
800   elegans. Elife. 2018;7. Epub 20180702. doi: 10.7554/eLife.36073. PubMed PMID: 29963981; PubMed
801   Central PMCID: PMCPMC6063732.

802   60.   White JG, Borisy GG. On the mechanisms of cytokinesis in animal cells. J Theor Biol.
803   1983;101(2):289-316. doi: 10.1016/0022-5193(83)90342-9. PubMed PMID: 6683772.

804   61.   Huang J, Huang Y, Yu H, Subramanian D, Padmanabhan A, Thadani R, et al. Nonmedially
805   assembled F-actin cables incorporate into the actomyosin ring in fission yeast. J Cell Biol.
806   2012;199(5):831-47. Epub 2012/11/28. doi: 10.1083/jcb.201209044. PubMed PMID: 23185032; PubMed
807   Central PMCID: PMCPMC3514790.

808   62.   Pelham RJ, Chang F. Actin dynamics in the contractile ring during cytokinesis in fission yeast.
809   Nature. 2002;419(6902):82-6. doi: 10.1038/nature00999. PubMed PMID: 12214236.

810   63.   Madrid M, Gómez-Gil E, Cansado J. Negative control of cytokinesis by stress-activated MAPK
811   signaling. Curr Genet. 2021;67(5):715-21. Epub 20210331. doi: 10.1007/s00294-021-01155-6. PubMed
812   PMID: 33791858.

813   64.   Malla M, Pollard TD, Chen Q. Counting actin in contractile rings reveals novel contributions of
814   cofilin and type II myosins to fission yeast cytokinesis. Mol Biol Cell. 2021:mbcE21080376. Epub
815   20211006. doi: 10.1091/mbc.E21-08-0376. PubMed PMID: 34613787.

816   65.   Bays JL, Campbell HK, Heidema C, Sebbagh M, DeMali KA. Linking E-cadherin
817   mechanotransduction to cell metabolism through force-mediated activation of AMPK. Nat Cell Biol.
818   2017;19(6):724-31. Epub 20170529. doi: 10.1038/ncb3537. PubMed PMID: 28553939; PubMed Central
819   PMCID: PMCPMC5494977.

820   66.   Shiraishi T, Verdone JE, Huang J, Kahlert UD, Hernandez JR, Torga G, et al. Glycolysis is the
821   primary bioenergetic pathway for cell motility and cytoskeletal remodeling in human prostate and
822   breast cancer cells. Oncotarget. 2015;6(1):130-43. doi: 10.18632/oncotarget.2766. PubMed PMID:
823   25426557; PubMed Central PMCID: PMCPMC4381583.

824   67.   DeWane G, Salvi AM, DeMali KA. Fueling the cytoskeleton - links between cell metabolism and
825   actin remodeling. J Cell Sci. 2021;134(3). Epub 20210208. doi: 10.1242/jcs.248385. PubMed PMID:
826   33558441; PubMed Central PMCID: PMCPMC7888749.

827   68.   Kim DU, Hayles J, Kim D, Wood V, Park HO, Won M, et al. Analysis of a genome-wide set of gene
828   deletions in the fission yeast Schizosaccharomyces pombe. Nat Biotechnol. 2010;28(6):617-23. Epub
829   20100516. doi: 10.1038/nbt.1628. PubMed PMID: 20473289; PubMed Central PMCID:
830   PMCPMC3962850.

831   69.   Hentges P, Van Driessche B, Tafforeau L, Vandenhaute J, Carr AM. Three novel antibiotic marker
832   cassettes for gene disruption and marker switching in Schizosaccharomyces pombe. Yeast.
833   2005;22(13):1013-9. doi: 10.1002/yea.1291. PubMed PMID: 16200533.

834   70.   Sato M, Dhut S, Toda T. New drug-resistant cassettes for gene disruption and epitope tagging in
835   Schizosaccharomyces pombe. Yeast. 2005;22(7):583-91. Epub 2005/06/09. doi: 10.1002/yea.1233.
836   PubMed PMID: 15942936.

837   71.   Petersen J, Russell P. Growth and the Environment of Schizosaccharomyces pombe. Cold Spring
838   Harb Protoc. 2016;2016(3):pdb.top079764. Epub 2016/03/05. doi: 10.1101/pdb.top079764. PubMed
839   PMID: 26933253; PubMed Central PMCID: PMCPMC5526333.

840   72.   Keeney JB, Boeke JD. Efficient targeted integration at leu1-32 and ura4-294 in
841   Schizosaccharomyces pombe. Genetics. 1994;136(3):849-56. doi: 10.1093/genetics/136.3.849. PubMed
842   PMID: 8005439; PubMed Central PMCID: PMCPMC1205890.

843   73.   Prieto-Ruiz F, Vicente-Soler J, Franco A, Gomez-Gil E, Sanchez-Marinas M, Vazquez-Marin B, et
844   al. RNA-Binding Protein Rnc1 Regulates Cell Length at Division and Acute Stress Response in Fission
845   Yeast through Negative Feedback Modulation of the Stress-Activated Mitogen-Activated Protein Kinase
846   Pathway. mBio. 2020;11(1). Epub 2020/01/09. doi: 10.1128/mBio.02815-19. PubMed PMID: 31911490;
847   PubMed Central PMCID: PMCPMC6946801.

848   74.   Moreno S, Klar A, Nurse P. Molecular Genetic-Analysis Of Fission Yeast Schizosaccharomyces
849   pombe. Methods in Enzymology. 1991;194:795-823. PubMed PMID: WOS:A1991FN84200056.

850   75.   Schneider C, Rasband W, Eliceiri K. NIH Image to ImageJ: 25 years of image analysis. Nature
851   Methods. 2012;9(7):671-5. doi: 10.1038/nmeth.2089. PubMed PMID: WOS:000305942200020.

852   76.   Grallert A, Hagan IM. Preparation of Protein Extracts from Schizosaccharomyces pombe Using
853   Trichloroacetic Acid Precipitation. Cold Spring Harb Protoc. 2017;2017(2). Epub 2017/02/01. doi:
854   10.1101/pdb.prot091579. PubMed PMID: 28148851.

855
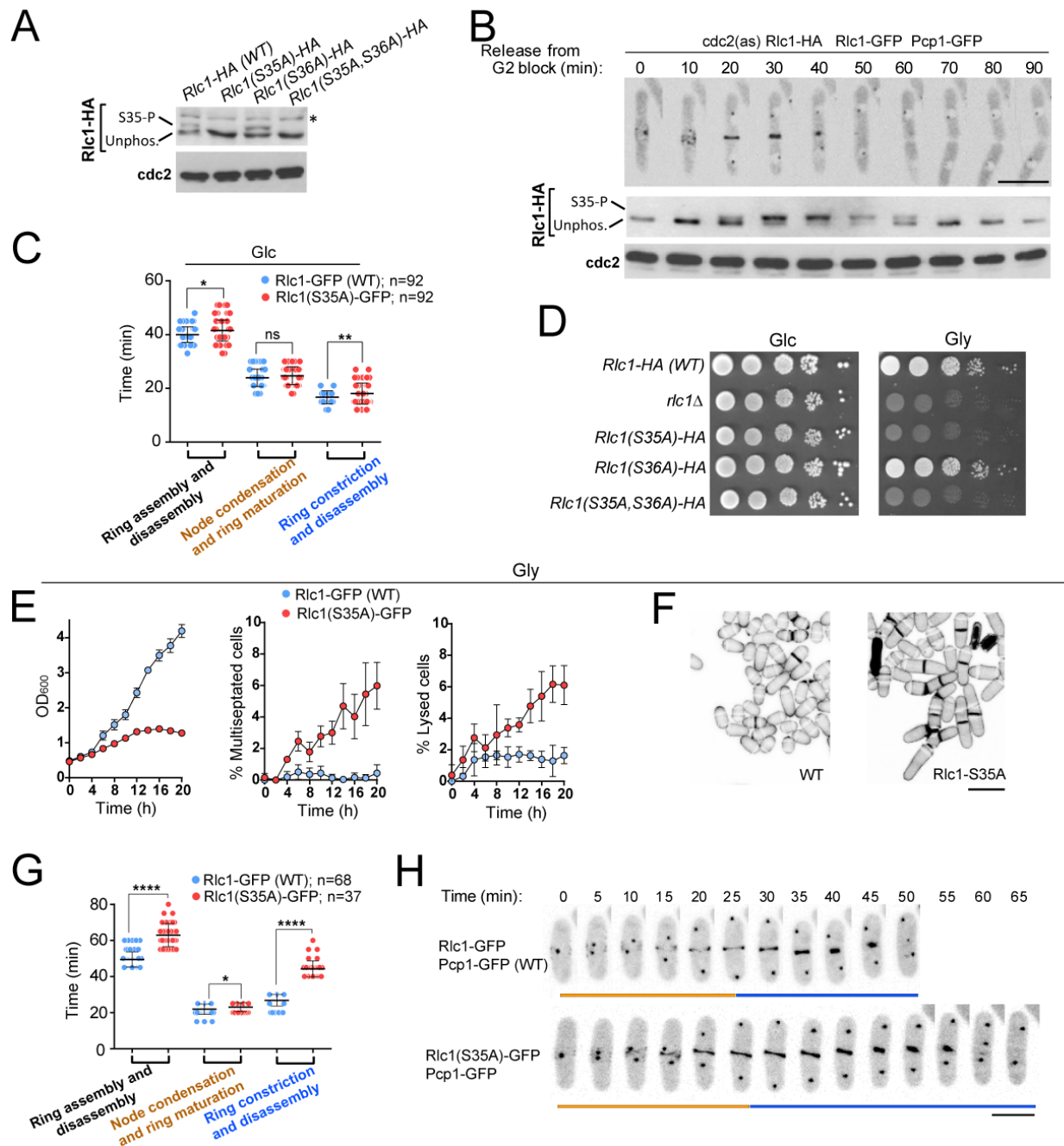
Figure 1. Myosin-II regulatory light chain phosphorylation is essential for *S. pombe* cytokinesis and growth during respiration.

(**A**) Total protein extracts from the indicated strains growing exponentially in YES-Glucose medium were resolved by SDS-PAGE, and the Rlc1-HA fusion was detected by incubation with anti-HA antibody. Anti-Cdc2 was used as a loading control. Rlc1 isoforms, phosphorylated (S35-P), and not phosphorylated at Ser35 (Unphos), are indicated. The blot corresponds to a representative experiment that was repeated at least three times with identical results. (**B**) Cells with *cdc2-asM17* analog-sensitive mutant allele co-

856

857
858
859
860
861
862
863

864   expressing Rlc1-HA and Rlc1-GFP genomic fusions were arrested at G2 in YES-Glucose medium

865   supplemented with 3-NM-PP1 and incubated in the same medium lacking the kinase analogue for the

866   indicated times. Time-lapse images of a representative cell showing Rlc1-GFP localization and mitotic

867   progression monitored using Pcp1-GFP marked SPBs (upper panel) (scale bar: 10 μm), and Western blot

868   analysis of Rlc1-HA mobility after release from the G2 block (lower panels), are shown. The Western

869   blot image corresponds to a representative experiment that was repeated at least three times with identical

870   results. (**C**) Times for ring assembly and disassembly, node condensation/ring maturation, and ring

871   constriction and disassembly were estimated for the indicated strains growing exponentially in YES-

872   Glucose medium (Glc), by time-lapse confocal fluorescence microscopy. *n* is the total number of cells

873   scored from three independent experiments, and data are presented as mean ± SD. Statistical comparison

874   between two groups was performed by unpaired Student's *t*-test. **, $p<0.005$; *, $p<0.05$; ns, not

875   significant, as calculated by unpaired Student's *t* test. (**D**) Decimal dilutions of strains of the indicated

876   genotypes were spotted on solid plates with YES-Glucose (Glc), or YES-Glycerol (Gly), incubated at

877   30°C for 3 (glucose plates) or 5 days (glycerol plates), and photographed. The image corresponds to a

878   representative experiment that was repeated at least three times with similar results. (**E**) The indicated

879   strains were grown in YES-Glucose to a final $OD_{600}=0.2$ and shifted to YES-Glycerol and incubated at

880   28°C. The OD_{600} value, and the percentage of multiseptated and lysed cells were quantified in aliquots

881   taken at the indicated times. Data correspond to three independent growth curves and are presented as

882   mean ± SD. (**F**) Representative maximum projection confocal images of cells growing for 12 h in YES-

883   Glycerol after cell-wall staining with calcofluor white. Scale bar: 10 μm (**G**) The times for total ring

884   assembly and disassembly, node condensation/ring maturation, and ring constriction were estimated for

885   the indicated strains cells growing exponentially in YES-Glycerol medium by time-lapse confocal

886   fluorescence microscopy. Mitotic progression was monitored using Pcp1-GFP-marked SPBs. *n* is the total

887   number of cells scored from three independent experiments, and data are presented as mean ± SD.

888   Statistical comparison between two groups was performed by unpaired Student's *t*-test. ****, $p<0.0001$;

889   *, $p<0.05$, as calculated by unpaired Student's *t*-test. (**H**) Representative maximum-projection time-lapse

890   images of Rlc1 dynamics at the equatorial region of cells growing YES-Glycerol. Mitotic progression was

891   monitored using Pcp1-GFP-marked SPBs. Time interval is 5 min. Scale bar: 10 μm.

892
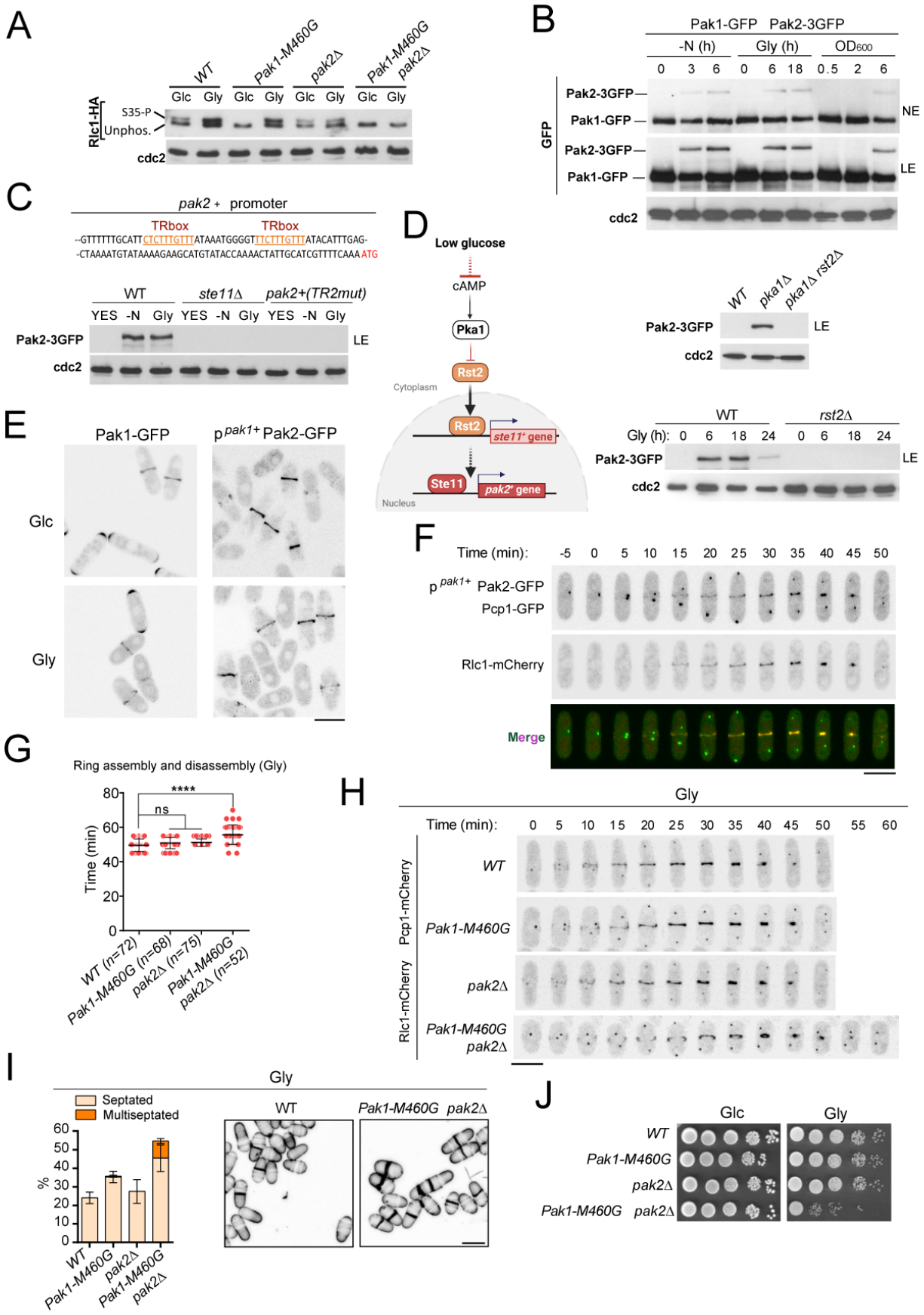
Figure 2. p21/Cdc42-activated kinase Pak2 phosphorylates Rlc1 at Ser35 together with Pak1 to

894 **positively control fission yeast cytokinesis and division during respiratory growth.**

895 (**A**) Total protein extracts from strains of the indicated genotypes growing exponentially in YES-Glucose

896 (Glc) or YES-Glycerol (Gly), were resolved by SDS-PAGE, and the Rlc1-HA fusion was detected by

897 incubation with anti-HA antibody. Anti-Cdc2 was used as a loading control. Rlc1 isoforms,

898 phosphorylated (S35-P), and not phosphorylated at Ser35 (Unphos), are indicated. The image corresponds

899 to a representative experiment that was repeated at least three times with similar results. (**B**) Glucose-

900 growing cells of a *S. pombe* strain co-expressing Pak1-GFP and Pak2-3GFP genomic fusions were

901 starved from nitrogen (-N), incubated in YES-Glycerol for the indicated times, or incubated in YES-

902 Glucose medium until reaching the indicated OD_{600} values. The corresponding total protein extracts were

903 resolved by SDS-PAGE, and Pak1-GFP and Pak2-3GFP fusions were detected by incubation with anti-

904 GFP antibody. Anti-Cdc2 was used as a loading control. The image corresponds to a representative

905 experiment that was repeated at least three times with identical results. NE: bands observed after 5 min

906 film exposure. LE: immunoreactive bands observed after an extended film exposure of 25 min. (**C**)

907 Upper: Partial nucleotide sequence of the promoter region of the *pak2+* gene. The two putative TR boxes

908 (Ste11-binding motifs) are shown in color. Lower: Western blot analysis of Pak2-3GFP levels in wild-

909 type, *ste11Δ*, and a mutant strain were the conserved G in the two putative TR boxes in the promoter of

910 *pak2+* gene was replaced by A, growing in YES-Glucose, after nitrogen starvation (-N), and a shift to

911 YES-Glycerol (Gly) for 12 h. Pak2-3GFP was detected by incubation with anti-GFP antibody, while anti-

912 Cdc2 was used as a loading control. The image corresponds to a representative experiment that was

913 repeated at least three times with identical results. (**D**) Left: Pak2 expression increases specifically during

914 respiratory growth in a Rst2- and Ste11-dependent manner in absence of cAMP-PKA signaling. See text

915 for a detailed description of its main components and functions. Upper right: total protein extracts from

916 strains of the indicated genotypes growing exponentially in YES-Glucose were resolved by SDS-PAGE,

917 and the Pak2-3GFP fusion was detected by incubation with anti-GFP antibody. Anti-Cdc2 was used as a

918 loading control. The image corresponds to a representative experiment that was repeated at least three

919 times with identical results. Lower right: total protein extracts from strains growing exponentially in

920 YES-Glycerol (Gly) for the indicated times were resolved by SDS-PAGE, and the Pak2-3GFP fusion was

921 detected by incubation with anti-GFP antibody. Anti-Cdc2 was used as a loading control. The image

922 corresponds to a representative experiment that was repeated at least three times with identical results. (**E**)

923 Representative maximum projection confocal images of exponentially growing cells from Pak1-GFP and

924 p^{pak1+}-Pak2-GFP cells growing exponentially in YES-Glucose (Glc), or YES-Glycerol (Gly). (**F**)

925 Representative maximum-projection time-lapse images of Pak2 and Rlc1 dynamics at the CAR in cells

926 co-expressing p^{pak1+}-Pak2-GFP and Rlc1-mCherry genomic fusions and growing in YES-Glycerol.

927   Mitotic progression was monitored using Pcp1-GFP-marked SPBs. Time interval is 5 min. (**G**) The total

928   time for ring assembly and disassembly was estimated for the indicated strains growing exponentially in

929   YES-Glycerol medium by time-lapse confocal fluorescence microscopy. Mitotic progression was

930   monitored using Pcp1-GFP-marked SPBs. *n* is the total number of cells scored from three independent

931   experiments, and data are presented as mean ± SD. Statistical comparison between groups was performed

932   by one-way ANOVA. ****, $p<0.0001$; ns, not significant. (**H**) Representative maximum-projection time-

933   lapse images of Rlc1 dynamics at the equatorial region in cells growing YES-Glycerol. Mitotic

934   progression was monitored using Pcp1-GFP-marked SPBs. Time interval is 5 min. Scale bar: 10 μm. (**I**)

935   Left: strains were grown in YES-Glycerol for 12 h, and the percentage of septated and multiseptated cells

936   were quantified. Data correspond to three independent experiments, and are presented as mean ± SD.

937   Right: representative maximum projection confocal images of cells from the indicated strains after cell-

938   wall staining with calcofluor white. (**J**) Decimal dilutions of strains of the indicated genotypes were

939   spotted on plates with YES-Glucose or YES-Glycerol, incubated at 30°C or 5 days, and photographed.

940   The image corresponds to a representative experiment that was repeated at least three times with similar

941   results.

942
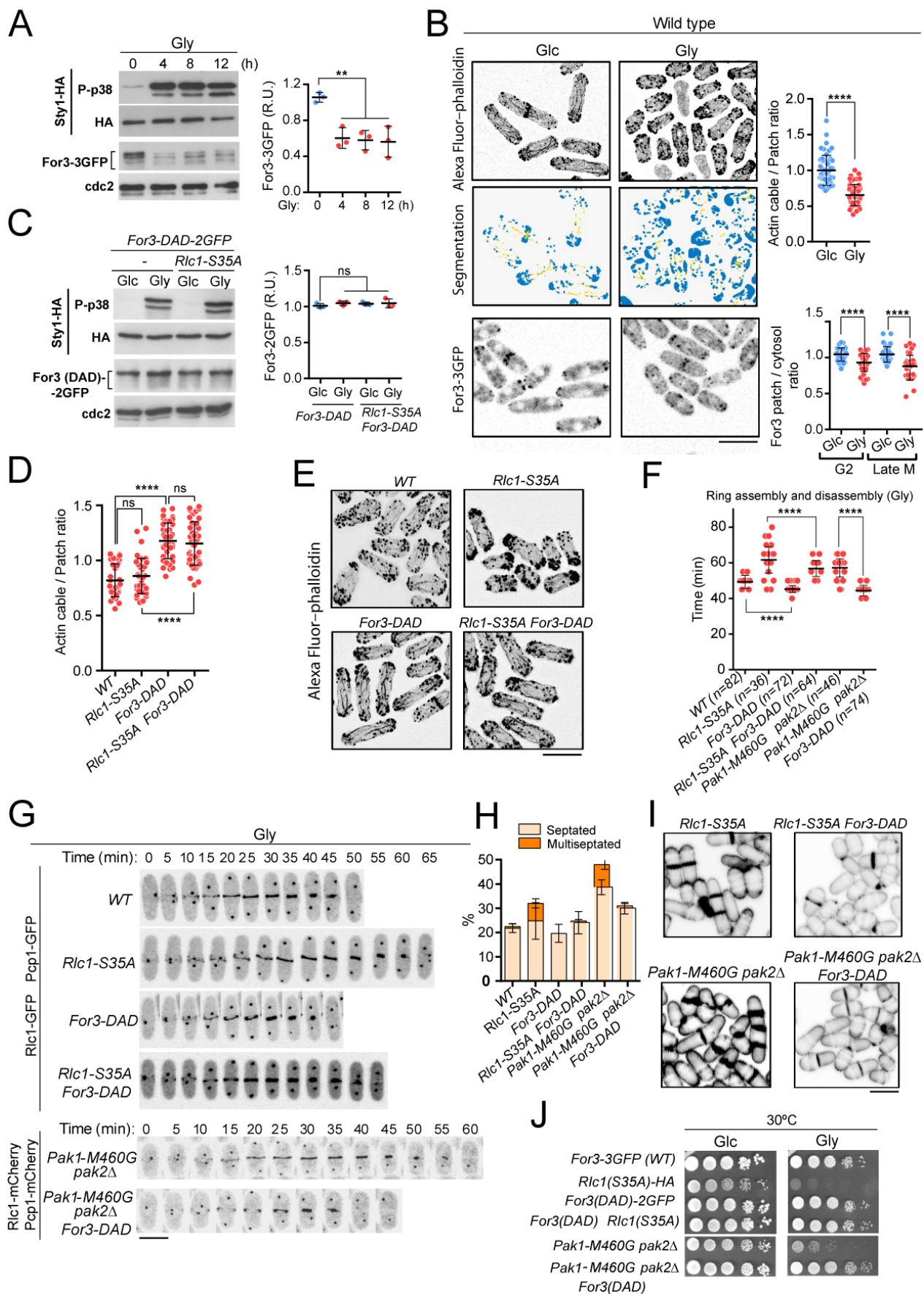
943 **Figure 3. PAK phosphorylation of Rlc1 is critical for *S. pombe* cytokinesis during respiration due to**

impaired For3-dependent actin cable nucleation imposed by SAPK activation.

(**A**) Left: *S. pombe* cells expressing genomic Sty1-HA and For3-3GFP fusions were grown in YES-Glucose to mid-log phase and transferred to YES-Glycerol medium for the indicated times. Activated/total Sty1 were detected with anti-phospho-p38 and anti-HA antibodies, respectively. Total For3 levels were detected with anti-GFP antibody. Anti-Cdc2 was used as a loading control. Right: For3 expression levels are represented as mean relative units ± SD and correspond to experiments performed as biological triplicates. **, p<0.005, as calculated by unpaired Student's *t*-test. (**B**) Upper: representative maximum projection images of Alexa Fluor–phalloidin stained *S. pombe* cells growing in YES-Glucose medium (Glc), or in YES-Glycerol (Gly) for 12 h. Segmentation analysis with Ilastik routine is shown below each image. Quantification data correspond to the actin cable to patch ratio of G2 cells (n=51) growing with Glucose or Glycerol, and are represented as mean relative units ± SD. ****, p<0.0001, as calculated by unpaired Student's *t*-test. Lower: representative maximum projection images of *S. pombe* cells expressing a genomic For3-3GFP fusion growing in YES-Glucose medium or in YES-Glycerol for 12 h. Quantification data (mean relative units ± SD), correspond to the For3 patch to cytosol ratio of G2 and late M cells (n=36), growing with Glucose or Glycerol. ****, p<0.0001, as calculated by unpaired Student's *t*-test. Scale bar: 10 μm. (**C**) Left: *S. pombe* wild-type and *rlc1-S35A* strains expressing genomic Sty1-HA and For3 (DAD)-2GFP fusions were grown in YES-Glucose (Glc) to mid-log phase and transferred to YES-Glycerol medium (Gly) for 12 h. Activated/total Sty1 were detected with anti-phospho-p38 and anti-HA antibodies, respectively. Total For3 levels were detected with anti-GFP antibody. Anti-Cdc2 was used as a loading control. Right: For3 expression levels are represented as mean relative units ± SD and correspond to experiments performed as biological triplicates. ns, not significant, as calculated by unpaired Student's *t*-test. (**D**) Actin cable to patch ratio of G2 cells from the indicated strains growing in YES-Glycerol medium for 12 h. Quantification data (n=41 cells for each strain), are represented as mean relative units ± SD. ****, p<0.0001; ns, not significant, as calculated by unpaired Student's *t*-test. (**E**) Representative maximum projection images of Alexa Fluor–phalloidin stained *S. pombe* cells of the indicated strains growing in YES-Glycerol medium for 12 h. (**F**) The total time for ring assembly and disassembly was estimated for the indicated strains growing exponentially in YES-Glycerol medium by time-lapse confocal fluorescence microscopy. *n* is the total number of cells scored from three independent experiments, and data are presented as mean ± SD. ****, p<0.0001, as calculated by unpaired Student's *t*-test. (**G**) Representative maximum-projection time-lapse images of Rlc1 dynamics at the equatorial region in cells from the indicated strains growing in YES-Glycerol. Mitotic progression was monitored using Pcp1-GFP-marked SPBs. Time interval is 5 min. (H) The indicated strains were grown in YES-Glycerol liquid medium for 12 h, and the percentage of septated and

977   multiseptated cells were quantified. Data correspond to three independent experiments and are presented

978   as mean ± SD. (**I**) Representative maximum projection confocal images of cells from the indicated strains

979   after cell-wall staining with calcofluor white. (**J**) Decimal dilutions of strains of the indicated genotypes

980   were spotted on plates with YES-Glucose (Glc) or YES-Glycerol (Gly), incubated at 30°C or 5 days, and

981   photographed. The image corresponds to a representative experiment that was repeated at least three

982   times with similar results.

983
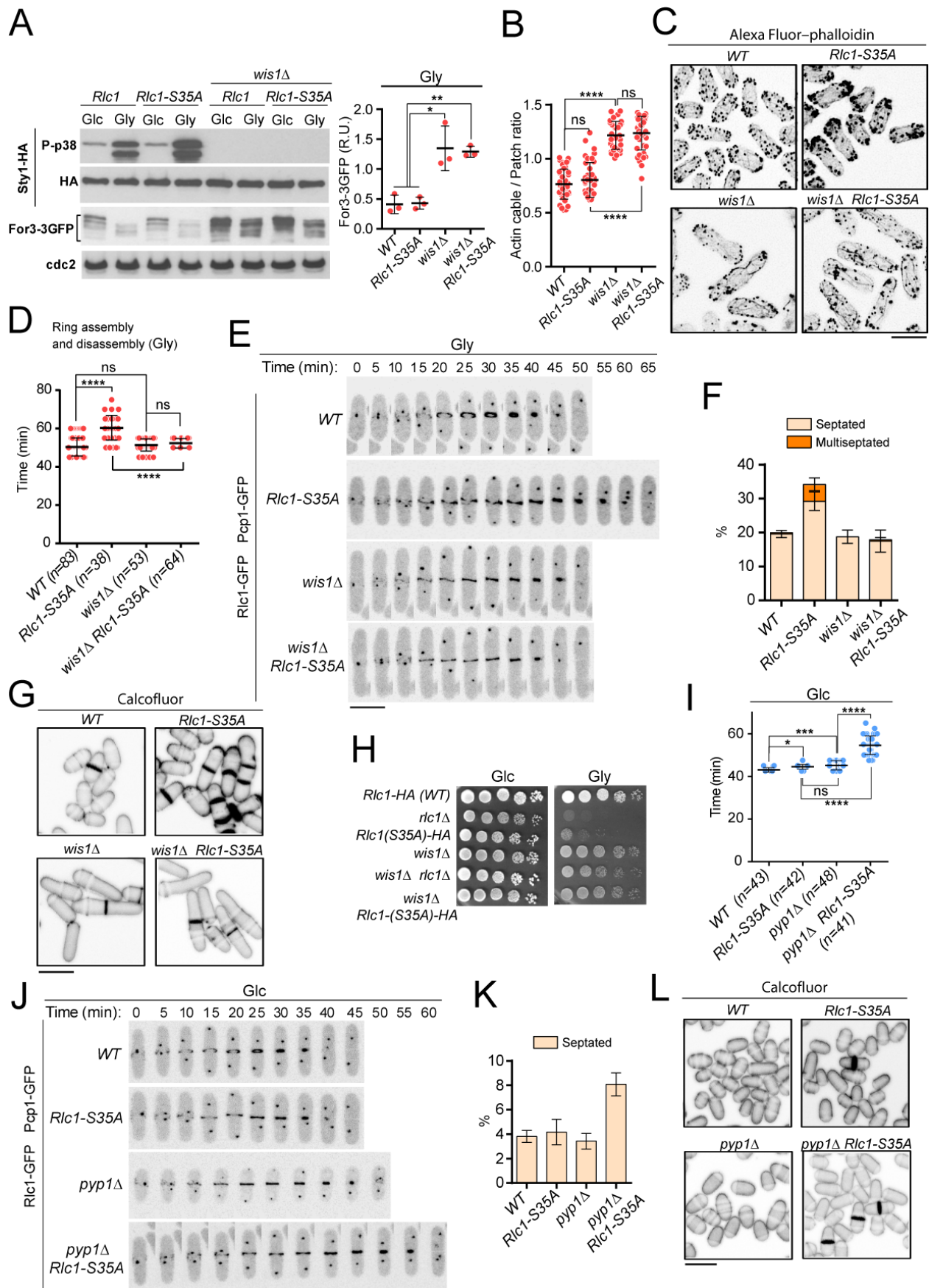
Figure 4. Lack of SAPK signaling restores *S. pombe* cytokinesis and growth during respiration in absence of Rlc1 phosphorylation.

(**A**) Left: *S. pombe* strains of the indicated genotypes expressing genomic Sty1-HA and For3-3GFP fusions were grown in either YES-Glucose (Glc) or YES-Glycerol (Gly) medium for 12 h. Activated/total Sty1 were detected with anti-phospho-p38 and anti-HA antibodies, respectively. Total For3 levels were detected with anti-GFP antibody. Anti-Cdc2 was used as a loading control. Right: For3 expression levels in glycerol-growing strains (Gly) are represented as mean relative units ± SD and correspond to experiments performed as biological triplicates. *, p<0.05; **, p<0.005, as calculated by unpaired Student's *t*-test. (**B**) Actin cable to patch ratio of G2 cells from the indicated strains growing in YES-Glycerol medium for 12 h. Quantification data (n=41 cells for each strain), are represented as mean relative units ± SD. ****, p<0.0001; ns, not significant, as calculated by unpaired Student's *t*-test. (**C**) Representative maximum projection images of Alexa Fluor–phalloidin stained *S. pombe* cells of the indicated strains growing in YES-Glycerol medium for 12 h. Scale bar: 10 μm. (**D**) The total time for ring assembly and disassembly was estimated for the indicated strains growing exponentially in YES-Glycerol medium by time-lapse confocal fluorescence microscopy. *n* is the total number of cells scored from three independent experiments, and data are presented as mean ± SD. ****, p<0.0001; ns, not significant, as calculated by unpaired Student's *t*-test. (**E**) Representative maximum-projection time-lapse images of Rlc1 dynamics at the equatorial region in cells from the indicated strains growing in YES-Glycerol. Mitotic progression was monitored using Pcp1-GFP-marked SPBs. Time interval is 5 min. (**F**) The indicated strains were grown in YES-Glycerol liquid medium for 12 h, and the percentage of septated and multiseptated cells were quantified. Data correspond to three independent experiments and are presented as mean ± SD. (**G**) Representative maximum projection confocal images of cells from the indicated strains after cell-wall staining with calcofluor white. (**H**) Decimal dilutions of strains of the indicated genotypes were spotted on plates with YES-Glucose or YES-Glycerol, incubated at 30°C or 5 days, and photographed. The image corresponds to a representative experiment that was repeated at least three times with similar results. (**I**) The total time for ring assembly and disassembly was estimated for the indicated strains growing exponentially in YES-Glucose medium by time-lapse confocal fluorescence microscopy. *n* is the total number of cells scored from three independent experiments, and data are presented as mean ± SD. ****, p<0.0001;***, p<0.001; *, p<0.05; ns, not significant, as calculated by unpaired Student's *t*-test. (**J**) Representative maximum-projection time-lapse images of Rlc1 dynamics at the equatorial region in cells from the indicated strains growing in YES-Glucose. Mitotic progression was monitored using Pcp1-GFP-marked SPBs. Time interval is 5 min. (**K**) The indicated strains were grown in YES-Glucose liquid medium, and the percentage of septated cells were quantified. Data correspond to

1018   three independent experiments and are presented as mean ± SD. (**L**) Representative maximum projection

1019   confocal images of cells from the indicated strains after cell-wall staining with calcofluor white.

1020
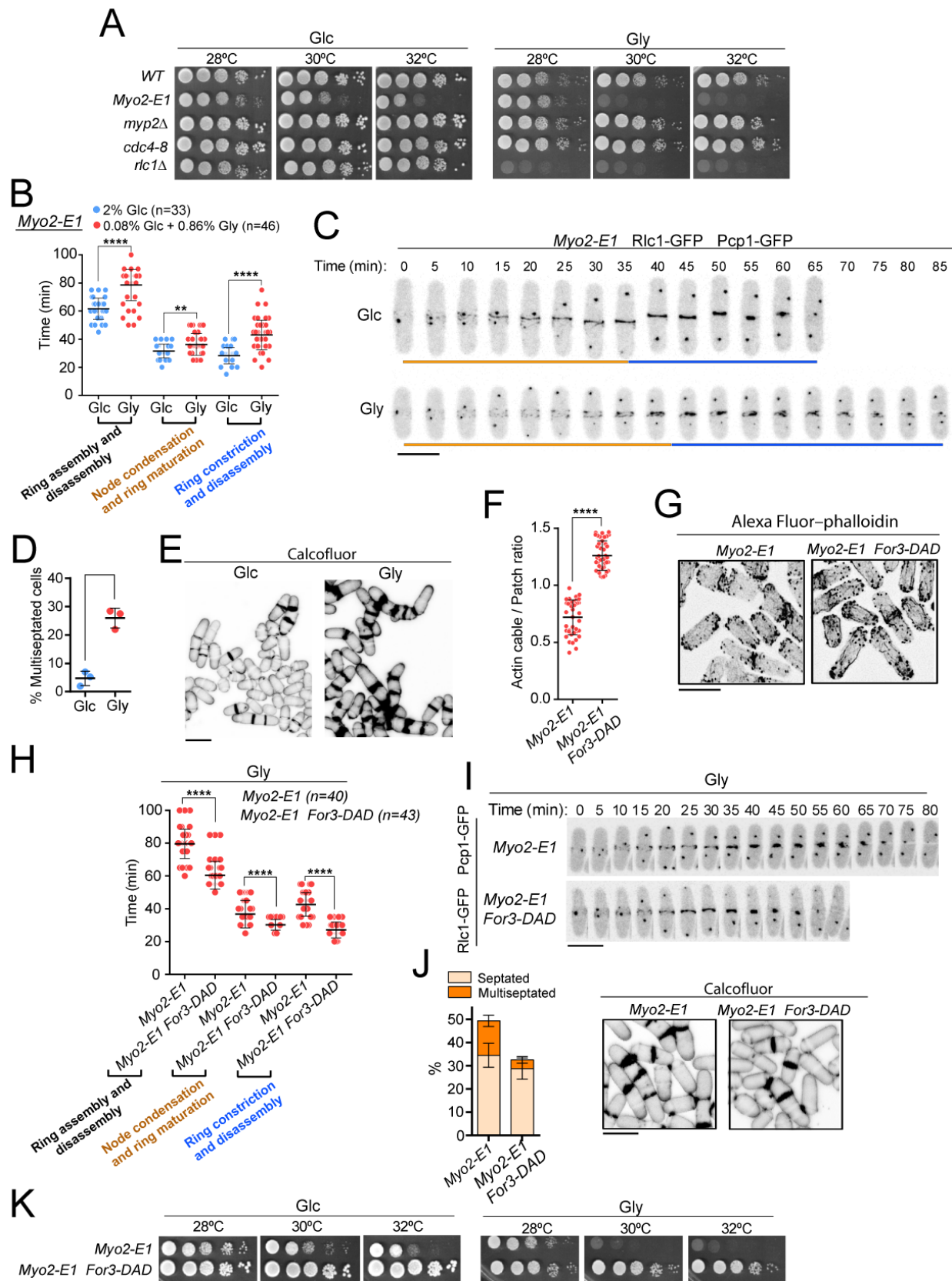
Figure 5. Control of Myo2 activity by Rlc1 phosphorylation regulates *S. pombe* cytokinesis and rowth during respiration.

(**A**) Decimal dilutions of strains of the indicated genotypes were spotted on plates with YES-Glucose or YES-Glycerol, incubated at 28, 30, and 32°C for 3 (Glc) or 5 (Gly) days, and photographed. The images correspond to a representative experiment that was repeated at least three times with similar results. (**B**) The times for ring assembly and disassembly, node condensation/ring maturation, and ring constriction and disassembly were estimated for *Myo2-E1* cells growing in YES-Glucose (Glc) and YES-Glycerol medium (Gly), by time-lapse confocal fluorescence microscopy. Mitotic progression was monitored using Pcp1-GFP-marked SPBs. *n* is the total number of cells scored from three independent experiments, and data are presented as mean ± SD. ****, p<0.0001; *, p<0.05, as calculated by unpaired Student's *t*-test. (**C**) Representative maximum-projection time-lapse images of Rlc1 dynamics at the equatorial region in *Myo2-E1* Rlc1-GFP cells growing in YES-Glucose (Glc) or YES-Glycerol (Gly). Mitotic progression was monitored using Pcp1-GFP-marked SPBs. Time interval is 5 min. Scale bar: 10 μm. (**D**) The percentage of multiseptated cells was quantified in *Myo2-E1* cells growing exponentially in YES-Glucose (Glc) or YES-Glycerol (Gly) for 12 h. Data correspond to three independent experiments, and are presented as mean ± SD. (**E**) Representative maximum projection confocal images of *Myo2-E1* cells growing in YES-Glucose or YES-Glycerol after cell-wall staining with calcofluor white. (**F**) Actin cable to patch ratio of G2 cells from the indicated strains growing in YES-Glycerol medium for 12 h. Quantification data (n=40 cells for each strain), are represented as mean relative units ± SD. ****, p<0.0001, as calculated by unpaired Student's *t*-test. (**G**) Representative maximum projection images of Alexa Fluor–phalloidin stained *S. pombe* cells of the indicated strains growing in YES-Glycerol medium for 12 h. (**H**) The times for ring assembly and disassembly, node condensation/ring maturation, and ring constriction and disassembly were estimated for *Myo2-E1* and *Myo2-E1 for3-DAD* cells growing exponentially in YES-Glycerol medium by time-lapse confocal fluorescence microscopy. Mitotic progression was monitored using Pcp1-GFP-marked SPBs. *n* is the total number of cells scored from three independent experiments, and data are presented as mean ± SD. Statistical comparison between two groups was performed by unpaired Student's *t*-test. ****, p<0.0001, as calculated by unpaired Student's *t* test. (**I**) Representative maximum-projection time-lapse images of Rlc1-GFP dynamics at the equatorial region in *Myo2-E1* and *Myo2-E1 for3-DAD* cells growing in YES-Glycerol. Mitotic progression was monitored using Pcp1-GFP-marked SPBs. Time interval is 5 min. (**J**) Left: the percentage of septated and multiseptated cells were quantified in *Myo2-E1* and *Myo2-E1 for3-DAD* cells growing for 12 h in YES-Glycerol medium. Data correspond to three independent experiments, and are presented as mean ± SD. Right: representative maximum projection confocal images after cell-wall staining with calcofluor white. (**K**) Decimal dilutions of strains of the indicated genotypes were spotted on plates with YES-Glucose or YES-Glycerol,

1055   incubated at 28, 30, and 32°C for 3 (Glc) or 5 (Gly) days, and photographed. The images correspond to a

1056   representative experiment that was repeated at least three times with similar results.

1057

1058

1059
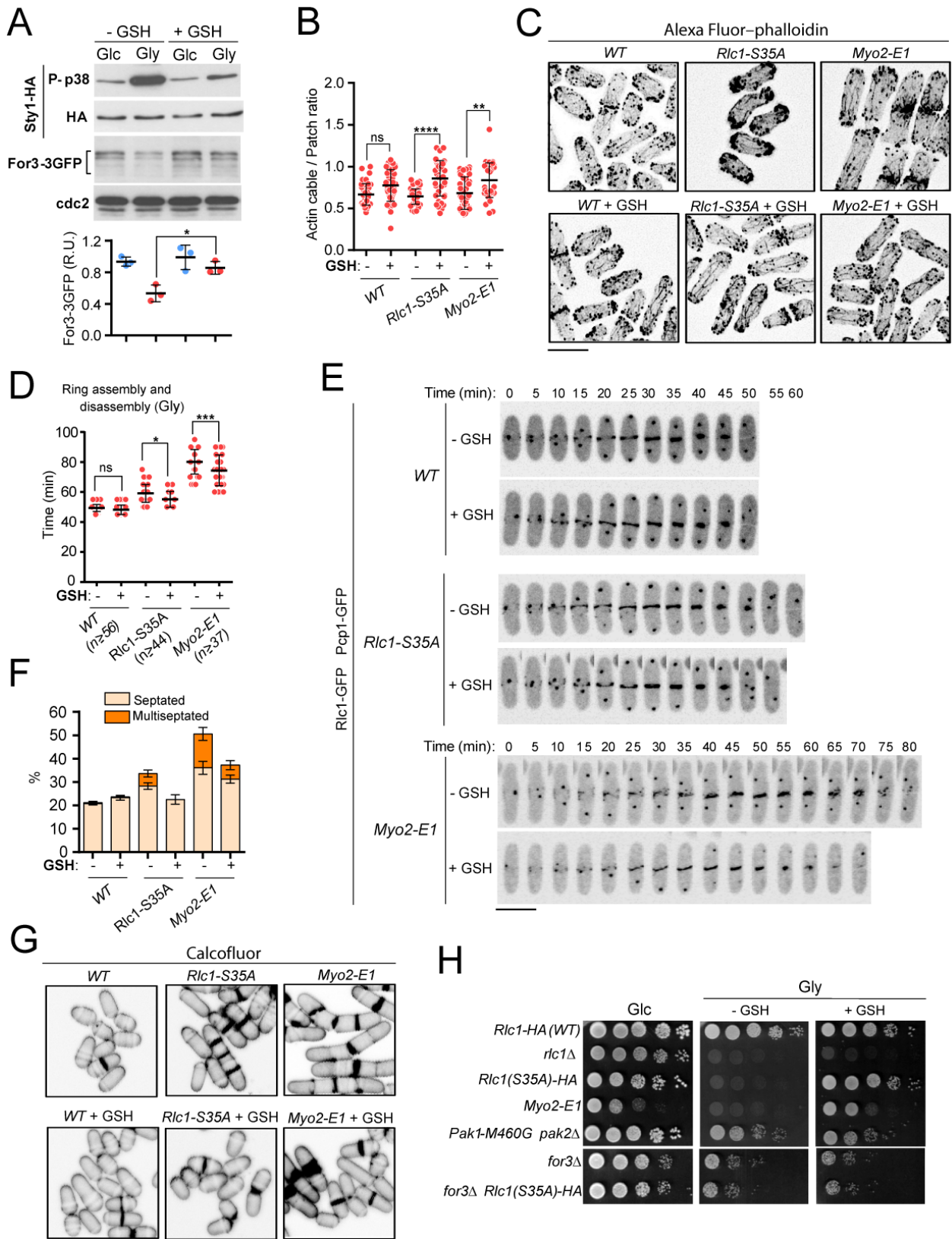
Figure 6. Exogenous antioxidants bypass the need for Rlc1 phosphorylation to regulate myosin II

activity and cytokinesis during respiratory growth.

1062 (**A**) Upper: *S. pombe* wild type cells expressing genomic Sty1-HA and For3-3GFP fusions were grown to
1063 mid-log phase in YES-Glucose (Glc) or YES-Glycerol (Gly), with or without 0.16 mM reduced
1064 glutathione (GSH). Activated/total Sty1 were detected with anti-phospho-p38 and anti-HA antibodies,
1065 respectively. Total For3 levels were detected with anti-GFP antibody. Anti-Cdc2 was used as a loading
1066 control. Lower: For3 expression levels are represented as mean relative units ± SD and correspond to
1067 experiments performed as biological triplicates. *, p<0.05, as calculated by unpaired Student's *t*-test. (**B**)
1068 Actin cable to patch ratio of G2 cells from the indicated strains growing in YES-Glycerol with or without
1069 0.16 mM GSH. Quantification data (n=41 cells for each strain), are represented as mean relative units
1070 ± SD. ****, p<0.0001; **, p<0.01; ns, not significant, as calculated by unpaired Student's *t*-test. (**C**)
1071 Representative maximum projection images of Alexa Fluor–phalloidin stained *S. pombe* cells of the
1072 indicated strains growing for 12 h in YES-Glycerol medium with or without 0.16 mM GSH. Scale bar: 10
1073 μm. (**D**) The total time for ring assembly and disassembly was estimated for the indicated strains growing
1074 exponentially in YES-Glycerol medium with or without 0.16 mM GSH by time-lapse confocal
1075 fluorescence microscopy. *n* is the total number of cells scored from three independent experiments, and
1076 data are presented as mean ± SD. ***, p<0.001; *, p<0.05 ns, not significant, as calculated by unpaired
1077 Student's *t* test. (**E**) Representative maximum-projection time-lapse images of Rlc1 dynamics at the
1078 equatorial region in cells from the indicated strains growing in YES-Glycerol with or without 0.16 mM
1079 GSH. Mitotic progression was monitored using Pcp1-GFP-marked SPBs. Time interval is 5 min. (**F**) The
1080 percentage of septated and multiseptated cells were quantified in the indicated strains growing for 12 h in
1081 YES-Glycerol medium with or without 0.16 mM GSH. Data correspond to three independent
1082 experiments, and are presented as mean ± SD. (**G**) Representative maximum projection confocal images
1083 of cells growing in YES-Glycerol after cell-wall staining with calcofluor white. (**H**) Decimal dilutions of
1084 strains of the indicated genotypes were spotted on plates with YES-Glucose or YES-Glycerol plates with
1085 or without 0.16 mM GSH, incubated at 28°C for 3 (Glc) or 5 (Gly) days, and photographed. The images
1086 correspond to a representative experiment that was repeated at least three times with similar results.

1087 **Supplemental Information for**

1088

1089 Myosin II regulatory light chain phosphorylation and formin availability modulate cytokinesis upon
1090 changes in carbohydrate metabolism.

1091

1092

1093 Francisco Prieto-Ruiz, Elisa Gómez-Gil, Rebeca Martín-García, Armando Jesús Pérez-Díaz, Jero
1094 Vicente-Soler, Alejandro Franco, Teresa Soto, Pilar Pérez, Marisa Madrid and José Cansado

1095

1096

1097 Corresponding authors: Marisa Madrid and José Cansado

1098

1099 Email: jcansado@um.es; marisa@um.es

1100

1101

1102

1103

1104
1105

1106

1107

1108

1109

1110

1111

1112

1113

1114

1115

1116

1117

1118

1119

1120

1121
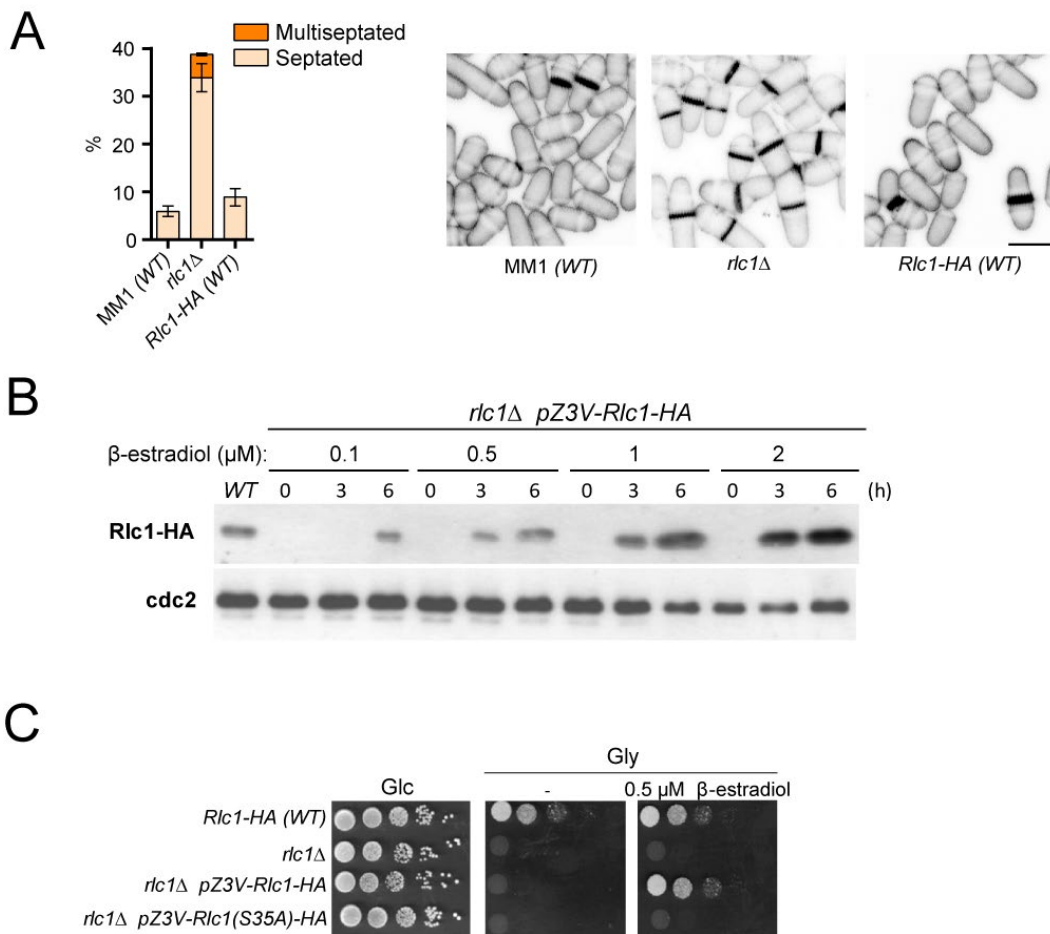
1122 **Figure 1—figure supplement 1. Rlc1 phosphorylation at Ser35 is essential for _S. pombe_ respiratory**
1123 **growth.**

1124 (**A**) Left: Strains of the indicated genotypes were grown in YES-Glucose liquid medium for 24 h, and the
1125 percentage of septated and multiseptated cells were quantified. Data correspond to three independent
1126 experiments, and are presented as mean ± SD. Right: representative maximum projection confocal images
1127 of cells from the indicated strains after cell-wall staining with calcofluor white. Scale bar: 10 μm.

1128 (**B**) The strain _rlc1Δ_ Z3EVpr:Rlc1-HA was grown in YES-Glucose medium to mid-log phase, and the
1129 culture was then treated with either 0.1, 0.5. 1, or 2 μM β-estradiol for 0, 3 and 6 h. Total extracts were
1130 resolved by SDS-PAGE, and Rlc1 levels were detected by incubation with anti-HA antibody. Anti-Cdc2
1131 was used as a loading control. The Western blot image corresponds to a representative experiment that
1132 was repeated at least three times with similar results.

1133 (**C**) Decimal dilutions of strains of the indicated genotypes were spotted on plates with YES-Glucose
1134 (Glc) or YES-Glycerol (Gly), with or without 0.5 μM β-estradiol, incubated at 30°C or 3 days, and
1135 photographed. The image corresponds to a representative experiment that was repeated at least three
1136 times with similar results.

44
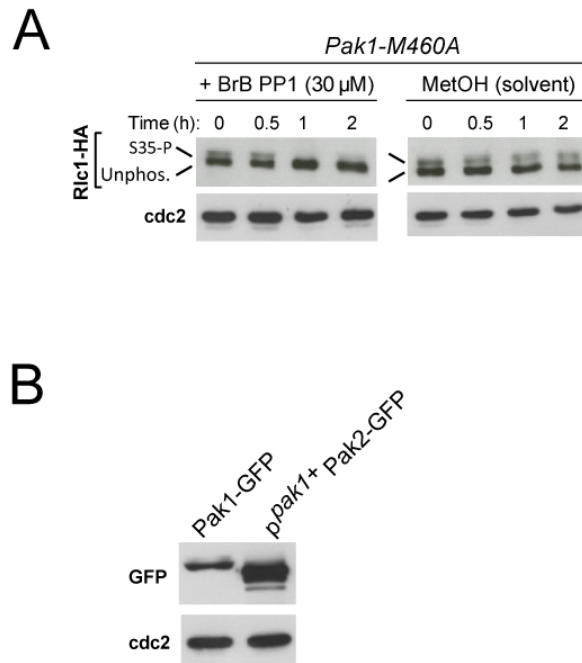
Figure 2—figure supplement 1. Pak1 phosphorylation of Rlc1 at Ser35 *in vivo*.

(**A**) Exponentially growing cells of the analog-sensitive strain Pak1-M460A were grown in YES-Glucose medium and treated with 30 µM of 3-BrB-PP1 for the indicated times, or remained untreated in the presence of solvent alone (MetOH). The corresponding protein extracts were resolved by SDS-PAGE, and the Rlc1-HA fusion was detected by incubation with anti-HA antibody. Anti-Cdc2 was used as a loading control. S35-P: Rlc1 isoform phosphorylated *in vivo* at Ser35. Unphos.: Rlc1 isoform not phosphorylated at Ser35. The image corresponds to a representative experiment that was repeated at least three times with similar results.

(**B**) Total protein extracts from strains expressing either Pak1-GFP or p*pak1+*-Pak2-GFP fusions and growing exponentially in YES-Glucose were resolved by SDS-PAGE. Fusions were detected by incubation with anti-GFP antibody. Anti-Cdc2 was used as a loading control. The image corresponds to a representative experiment that was repeated at least three times with similar results.
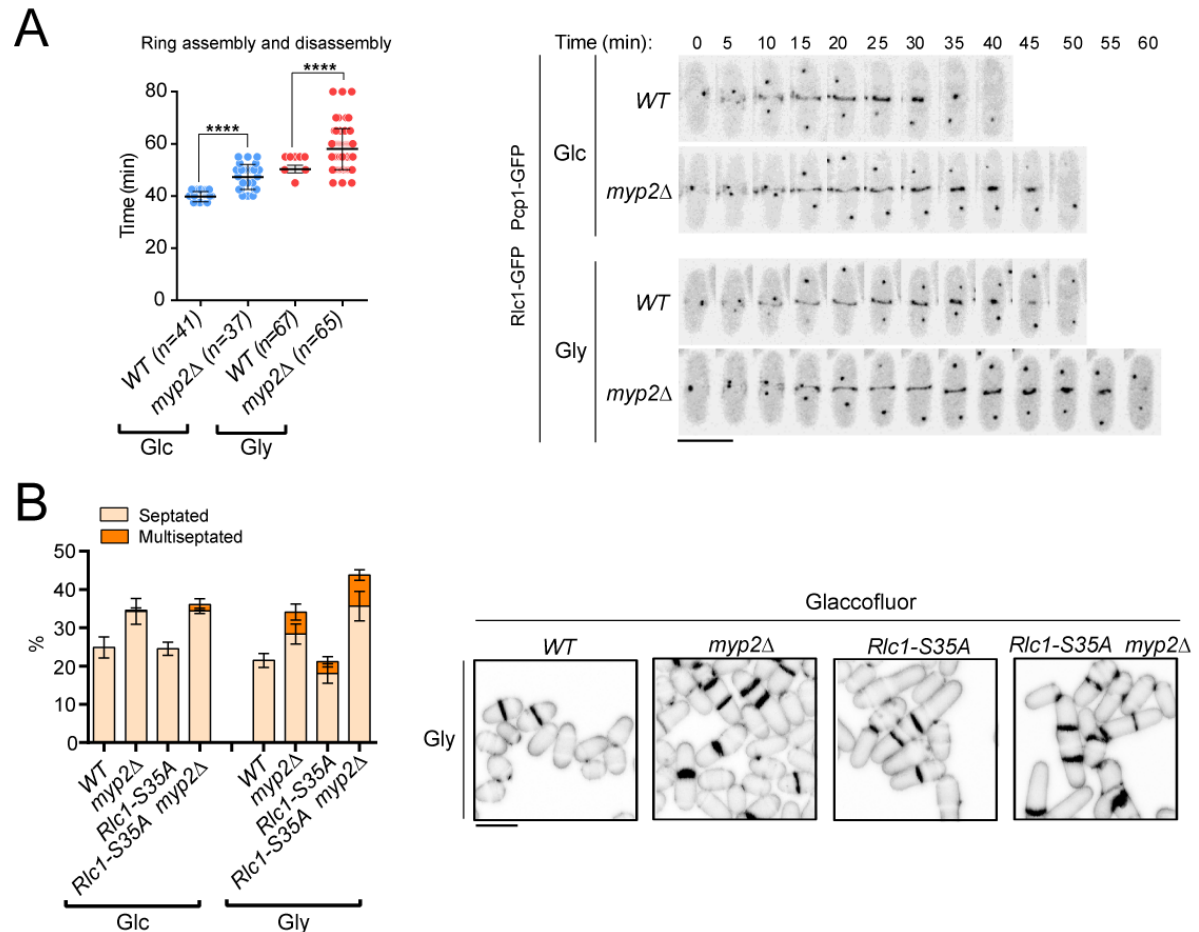
45

1169
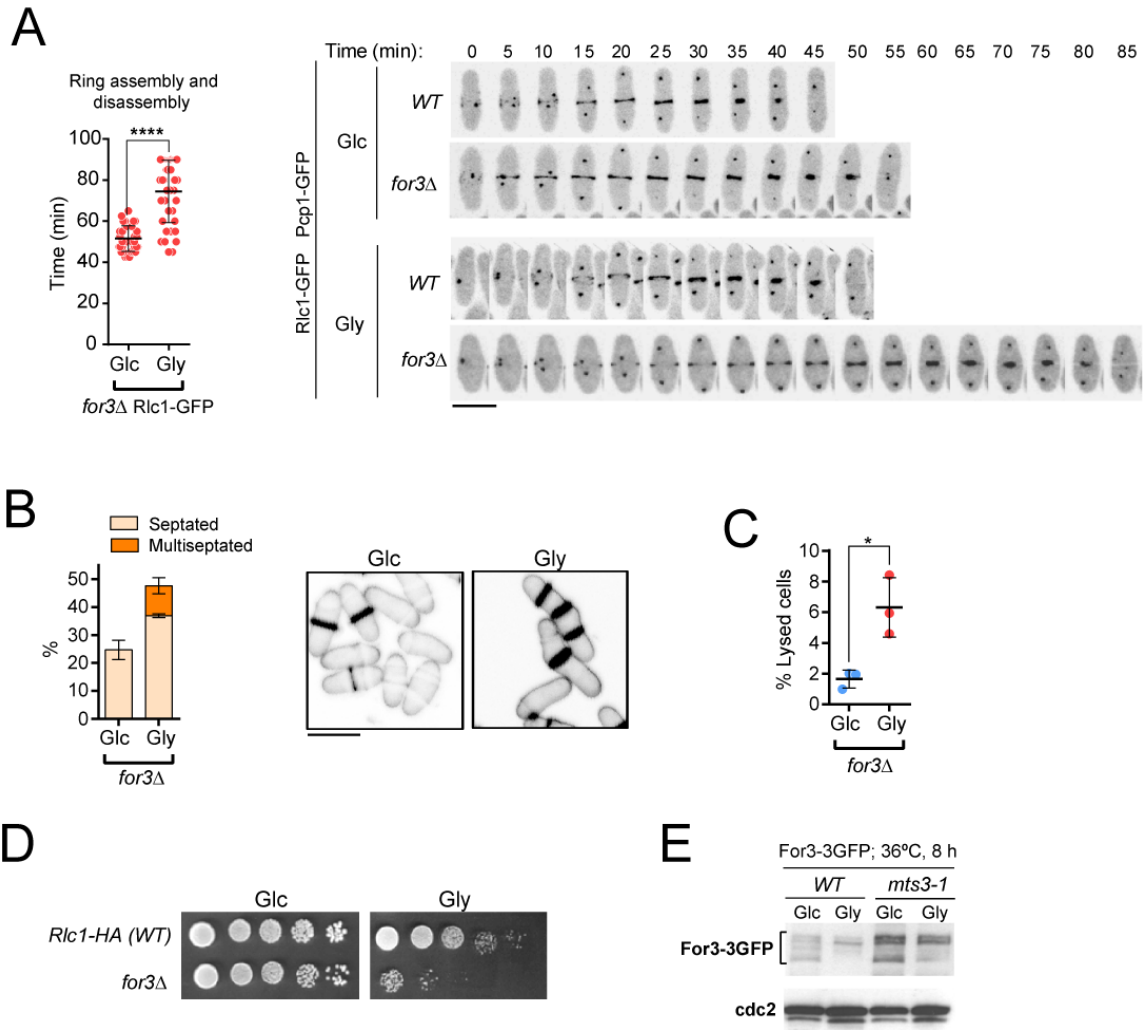
Figure 3—figure supplement 1. For3 formin is required for *S. pombe* cytokinesis during respiratory growth.

(**A**) Left: the total time for ring assembly and disassembly was estimated for *for3Δ* Rlc1-GFP cells growing exponentially in either YES-Glucose (Glc) or YES-Glycerol (Gly) medium by time-lapse confocal fluorescence microscopy. n≥36 cells from three independent experiments were scored in each condition, and data are presented as mean ± SD. ****, p<0.0001, as calculated by unpaired Student's *t* test. Right: representative maximum-projection time-lapse images of Rlc1 dynamics at the equatorial region in cells from the indicated strains growing in YES-Glucose or YES-Glycerol. Mitotic progression was monitored using Pcp1-GFP-marked SPBs. Time interval is 5 min. Scale bar: 10 μm.

(**B**) Left: the percentage of septated and multiseptated cells were quantified in *for3Δ* cells growing for 12 h in either YES-Glucose (Glc) or YES-Glycerol medium (Gly). Data correspond to three independent experiments, and are presented as mean ± SD. Right: representative maximum projection confocal images after cell-wall staining with calcofluor white. Scale bar: 10 μm.

(**C**) The percentage of cell lysis was quantified in *for3Δ* cells growing for 12 h in either YES-Glucose (Glc) or YES-Glycerol medium (Gly). Data correspond to three independent experiments, and are presented as mean ± SD. *, $p<0.05$, as calculated by unpaired Student's *t* test.

(**D**) Decimal dilutions of strains of the indicated genotypes were spotted on plates with YES-Glucose (Glc) or YES-Glycerol (Gly), incubated at 30°C for 5 days, and photographed. The image corresponds to a representative experiment that was repeated at least three times with similar results.

(**E**) For3-3GFP levels were determined by Western blot analysis with anti-GFP antibody in extracts from wild-type and the proteasome mutant *mts3-1* growing in YES-Glucose (Glc) or YES-Glycerol (Gly) and incubated at 36ºC for 8 h. Anti-Cdc2 was used as a loading control. The image corresponds to a representative experiment that was repeated at least three times with similar results.

1196

1197

1198

1199

1200

1201

1202

1203

1204

1205

1206
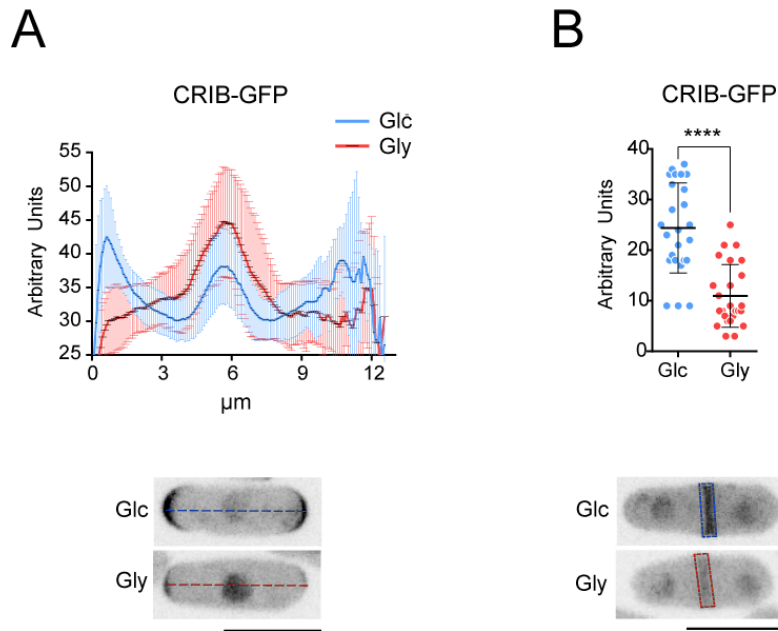
1207 **Figure 3—figure supplement 2**. **Localization of activated Ccd42 at the cell poles and the CAR is**
1208 **reduced during respiratory growth.**

1209 (**A**) Upper: intensity plots of CRIB-3GFP fusion (shown as arbitrary fluorescence units), were generated
1210 from line scans across the equatorial region of *S. pombe* G2 cells (n= 30) growing in YES-Glucose (Glc)
1211 or YES-Glycerol (Gly). Data are presented as mean ± SD. Lower: representative maximum-projection
1212 images of glucose and glycerol growing cells are shown. Scale bar: 10 µm.

1213 (**B**) Upper: the intensity of the CRIB-3GFP fusion at the medial region of dividing cells (n= 25) in YES-
1214 Glucose (Glc) or YES-Glycerol (Gly) was measured and is shown as arbitrary fluorescence units. Data
1215 are presented as mean ± SD. ****, p<0.0001, as calculated by unpaired Student's *t* test. Lower:
1216 representative maximum-projection images of dividing cells are shown. Scale bar: 10 µm.
1217

1223   **Figure 5—figure supplement 1. Role of Myp2 on *S. pombe* cytokinesis during respiration.**

1224   (**A**) Left: the times for ring assembly and disassembly, was estimated for wild type and *myp2Δ* cells
1225   growing in YES-Glucose (Glc) or YES-Glycerol medium (Gly), by time-lapse confocal fluorescence
1226   microscopy. Mitotic progression was monitored using Pcp1-GFP-marked SPBs. *n* is the total number of
1227   cells scored from three independent experiments, and data are presented as mean ± SD. Statistical
1228   comparison between two groups was performed by unpaired Student's *t* test. ****, p<0.0001, as
1229   calculated by unpaired Student's *t* test. Right: representative maximum-projection time-lapse images of
1230   Rlc1 dynamics at the equatorial region of wild type and *myp2Δ* cells growing in YES-Glucose (Glc) or
1231   YES-Glycerol (Gly). Mitotic progression was monitored using Pcp1-GFP-marked SPBs. Time interval is
1232   5 min. Scale bar: 10 μm.

1233   (**B**) Left: the percentage of septated and multiseptated cells were quantified in the indicated strains
1234   growing for 12 h in YES-Glucose (Glc) or YES-Glycerol (Gly). Data correspond to three independent
1235   experiments, and are presented as mean ± SD. Right: representative maximum projection confocal images
1236   of cells growing in YES-Glycerol after cell-wall staining with calcofluor white. Scale bar: 10 μm.

1237
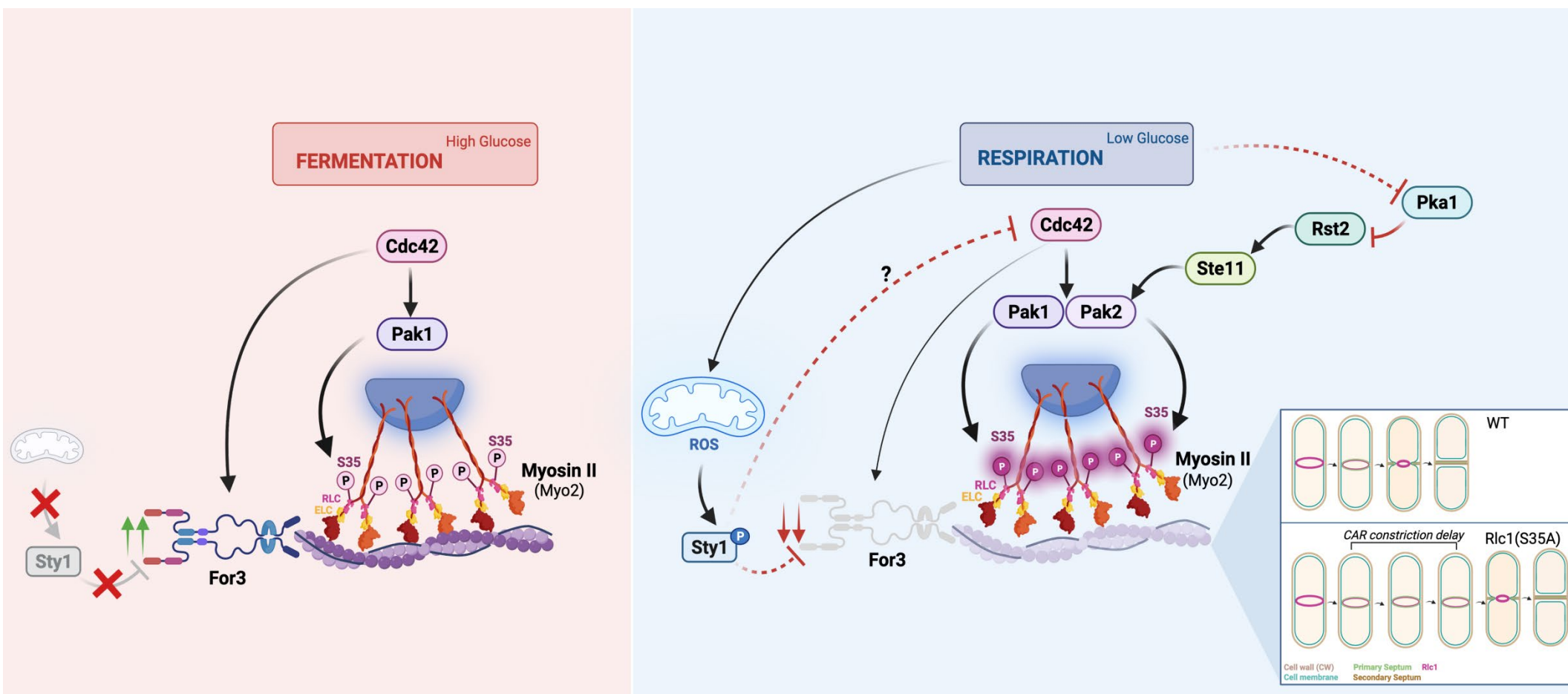
Figure 6—figure supplement 1. Model depicting the signaling pathways and mechanisms that regulate *S. pombe* cytokinesis by Myosin II (Myo2) through regulatory light chain phosphorylation during the transition from fermentative to respiratory metabolism. For specific details, please see text.

1 <u>**Source files legends**</u>

2

3 **Figure 1- source data 1.** Source data for Figure 1

4 **Figure 1- source data 2.** Western blot images for Figure 1 A,B

5 **Figure 1- figure supplement 1-source data 1.** Source data for Figure 1-figure supplement 1

6 **Figure 1- figure supplement 1- source data 2**. Western blot images for figure supplement 1B

7 **Figure 2- source data 1.** Source data for Figure 2

8 **Figure 2- source data 2.** Western blot images for Figure 2B,C,D.

9 **Figure 2- figure supplement 1- source data 1.** Western blot images for figure supplement 1A,B

10 **Figure 3- source data 1.** Source data for Figure 3

11 **Figure 3- source data 2.** Western blot images for Figure 3A,C.

12 **Figure 3- figure supplement 1-source data 1.** Source data for Figure 3-figure supplement 1

13 **Figure 3- figure supplement 1-source data 2.** Western blot images for figure supplement 1E

14 **Figure 3- figure supplement 2-source data 1.** Source data for Figure 3-figure supplement 2

15 **Figure 4- source data 1.** Source data for Figure 4

16 **Figure 4- source data 2.** Western blot images for Figure 4A.

17 **Figure 5- source data 1.** Source data for Figure 5

18 **Figure 5- figure supplement 1-source data 1.** Source data for Figure 5-figure supplement 1

19 **Figure 6- source data 1.** Source data for Figure 6

20 **Figure 6- source data 2.** Western blot images for Figure 6A.

21

22

23

24

Table S1. *S. pombe* strains used in this study.

Strain	Genotype	Source/Reference
	Figure 1	
FPR727	*h⁻ rlc1::kanR rlc1-HA::ura4⁺ ade6-M216 leu1-32*	This work
FPR645	*h⁻ rlc1::kanR ade6-M216 leu1-32 ura4.294*	This work
FPR730	*h⁻ rlc1::kanR rlc1(S35A)-HA::ura4⁺ ade6-M216 leu1-32*	This work
FPR732	*h⁻ rlc1::kanR rlc1(S36A)-HA::ura4⁺ ade6-M216 leu1-32*	This work
FPR735	*h⁻ rlc1::kaRn rlc1(S35AS36A)-HA::ura4⁺ ade6-M216 leu1-32*	This work
FPR830	*h? Pcp1-GFP:kanR Rlc1-GFP:kanR cdc2ASM17:bsdR rlc1-HA::ura4⁺ ade6-M216 leu1-32*	This work
FPR961	*h⁺ Pcp1-GFP:kanR rlc1::kanR Rlc1-GFP::ura4⁺ ade6-M216 leu1-32*	This work
FPR965	*h⁺ Pcp1-GFP:kanR rlc1::kanR Rlc1(S35A)-GFP::ura4⁺ ade6-M216 leu1-32*	This work
	Figure 2	
MBY4489	*h⁻ pak1-2xMyc-GFP::ura4⁺*	Loo *et al.,* 2008
MBY5064	*h⁻ pak1-M460G-2xMyc-GFP::ura4⁺*	Loo *et al.,* 2008
FPR1132	*h? pak1-2xMyc-GFP::ura4⁺ rlc1::kanR rlc1-HA::ura4⁺ ade6-M216 leu1-32*	This work
FPR1141	*h? pak1M460G-2xMyc-GFP::ura4⁺ rlc1::kanR rlc1-HA::ura4⁺ ade6-M216 leu1-32*	This work
FPR1145	*h? pak1-2xMyc-GFP::ura4⁺ rlc1::kanR shk2::kanR rlc1-HA::ura4⁺ ade6-M216 leu1-32*	This work
FPR1142	*h? pak1M460G-2xMyc-GFP::ura4⁺ rlc1::kanR shk2::kanR rlc1-HA::ura4⁺ ade6-M216 leu1-32*	This work
FPR1269	*h? pak1-2xMyc-GFP::ura4⁺ Pcp1-mcherry::ura4⁺ Rlc1-mcherry::kanR ade6-M216 leu1-32 ura4.D18*	This work
FPR1281	*h? pak1M460G-2xMyc-GFP::ura4⁺ Pcp1-mcherry::ura4⁺ Rlc1-mcherry::kanR ade6-M216 leu1-32 ura4.D18*	This work
FPR1272	*h? pak1-2xMyc-GFP::ura4⁺ Pcp1-mcherry::ura4⁺ Rlc1-mcherry::kanR shk2::kanR ade6-M216 leu1-32 ura4.D18*	This work
FPR1282	*h? pak1M460G-2xMyc-GFP::ura4⁺ Pcp1-mcherry::ura4⁺ Rlc1-mcherry::kanR shk2::kanR ade6-M216 leu1-32 ura4.D18*	This work
PPG4.69	*h⁺ pak1-GFP::kanR leu1-32 ura4.D18*	Lab
FPR1482	*h? pak1-GFP::kanR shk2::hphR shk2-3xGFP::ura4⁺ ade6-M216 leu1-32*	This work
FPR1460	*h⁻ shk2::hphR shk2-3xGFP::ura4⁺ ade6-M216 leu1-32*	This work
FPR1554	*h⁻ shk2::hphR shk2-3xGFP::ura4⁺ ste11::natR ade6-M216 leu1-32*	This work
FPR1481	*h⁻ shk2::hphR promste11⁺A/G:shk2-3xGFP::ura4⁺ ade6-M216 leu1-32*	This work
FPR1607	*h? shk2::hphR shk2-3xGFP::ura4⁺ pka1::kanR ade6-M216 leu1-32*	This work

FPR1608	*h? shk2::hphR shk2-3xGFP::ura4+ rst2::natR ade6-M216 leu1-32*	
FPR1611	*h? shk2::hphR shk2-3xGFP::ura4+ pka1::kanR rst2::natR ade6-M216 leu1-32*	
FPR1530	*h- shk2::hphR prompak1+shk2-GFP::ura4+ ade6-M216 leu1-32*	This work
FPR1559	*h? shk2::hphR prompak1+shk2-GFP::ura4+ pcp1-mcherry::ura4+ Rlc1-mcherry::kanR ade6-M216 leu1-32*	This work
	Figure 3	
E888	*h+ for3-3xGFP::ura4+ sty1-HA6H::ura4+ ade6-M216 leu1-32 ura4-D18*	Gomez-Gil *et al.*, 2020
FPR1441	*h? for3DAD-2xGFP::kanR sty1-HA6H::ura4+ rlc1::kanR rlc1-GFP::ura4+ ade6-M216 leu1-32 ura4-D18*	This work
FPR1443	*h? for3DAD-2xGFP::kanR sty1-HA6H::ura4+ rlc1::kanR rlc1(S35A)-GFP::ura4+ ade6-M216 leu1-32 ura4-D18*	This work
FPR961	*h+ Pcp1-GFP:kanR rlc1::kanR Rlc1-GFP::ura4+ ade6-M216 leu1-32*	This work
FPR965	*h+ Pcp1-GFP:kanR rlc1::kanR Rlc1(S35A)-GFP::ura4+ ade6-M216 leu1-32*	This work
FPR1292	*h? Pcp1-GFP:kanR rlc1::kanR Rlc1-GFP::ura4+ for3DAD ade6-M216 leu1-32*	This work
FPR1296	*h? Pcp1-GFP:kanR rlc1::kanR Rlc1(S35A)-GFP::ura4+ for3DAD ade6-M216 leu1-32*	This work
FPR1340	*h? Pcp1-mcherry::ura4+ Rlc1-mcherry::kanR for3-3xGFP::ura4+ pak1-M460G-2xMyc-GFP::ura4+ shk2::kanR ade6-M216 leu1-32 ura4.D18*	This work
FPR1345	*h? Pcp1-mcherry::ura4+ Rlc1-mcherry::kanR pak1-M460G-2xMyc-GFP::ura4+ for3DAD-2xGFP::kanR shk2::kanR ade6-M216 leu1-32 ura4.D18*	This work
FPR1089	*h? for3-3xGFP::ura4+ rlc1::kanR rlc1-HA::ura4+ kanR ade6-M216 leu1-32*	This work
FPR1094	*h? for3-3xGFP::ura4+ rlc1::kanR rlc1(S35A)-HA::ura4+ kanR ade6-M216 leu1-32*	This work
FPR1410	*h? for3DAD-2xGFP::kanR rlc1::kanR rlc1-HA::ura4+ kanR ade6-M216 leu1-32*	This work
FPR1415	*h? for3DAD-2xGFP::kanR rlc1::kanR rlc1(S35A)-HA::ura4+ kanR ade6-M216 leu1-32*	This work
	Figure 4	
FPR1000	*h+ for3-3xGFP::ura4+ sty1-HA6H::ura4+ rlc1::kanR rlc1-GFP::ura4+ ade6-M216 leu1-32*	This work
FPR1048	*h+ for3-3xGFP::ura4+ sty1-HA6H::ura4+ rlc1::kanR rlc1(S35A)-GFP::ura4+ ade6-M216 leu1-32*	This work
FPR1054	*h? for3-3xGFP::ura4+ sty1-HA6H::ura4+ rlc1::kanR rlc1-GFP::ura4+ wis1::his ade6-M216 leu1-32*	This work
FPR1059	*h? for3-3xGFP::ura4+ sty1-HA6H::ura4+ rlc1::kanR rlc1(S35A)-GFP::ura4+ wis1::his ade6-M216 leu1-32*	This work
FPR727	*h- rlc1::kanR rlc1-HA::ura4+ ade6-M216 leu1-32*	This work
FPR645	*h- rlc1::kanR ade6-M216 leu1-32 ura4.294*	This work

FPR730	*h⁻ rlc1::kanR rlc1(S35A)-HA::ura4⁺ ade6-M216 leu1-32*	This work
FPR1228	*h⁻ rlc1::kanR rlc1-HA::ura4⁺ wis1::his ade6-M216 leu1-32*	This work
FPR1231	*h⁻ rlc1::kanR wis1::his ade6-M216 leu1-32*	This work
FPR1237	*h⁻ rlc1::kanR rlc1(S35A)-HA::ura4⁺ wis1::his ade6-M216 leu1-32*	This work
FPR961	*h⁺ Pcp1-GFP:kanR rlc1::kanR Rlc1-GFP::ura4⁺ ade6-M216 leu1-32*	This work
FPR965	*h⁺ Pcp1-GFP:kanR rlc1::kanR Rlc1(S35A)-GFP::ura4⁺ ade6-M216 leu1-32*	This work
FPR1233	*h? Pcp1-GFP:kanR rlc1::kanR Rlc1-GFP::ura4⁺ wis1::his ade6-M216 leu1-32*	This work
FPR1235	*h? Pcp1-GFP:kanR rlc1::kanR Rlc1(S35A)-GFP::ura4⁺ wis1::his ade6-M216 leu1-32*	This work
FPR1361	*h? Pcp1-GFP:kanR rlc1::kanR Rlc1-GFP::ura4⁺ pyp1::kanR ade6-M216 leu1-32*	This work
FPR1406	*h? Pcp1-GFP:kanR rlc1::kanR Rlc1(S35A)-GFP::ura4⁺ pyp1::hphR ade6-M216 leu1-32*	This work
	<u>Figure 5</u>	
MM1	*h⁺ ade6-M216 leu1-32 ura4.D18*	Madrid *et al.*, 2006
FPR876	*h- myo2.E1 ade6-M216 leu1-32 ura4.D18*	Balasubramanian *et al.,* 1998
FPR462	*h⁺ myo3::kanR ade6-M216 leu1-32 ura4.D18*	Lab Stock
FPR441	*h⁺ cdc4-8 ade6-M216 leu1-32 ura4.D18*	Lab Stock
FPR645	*h⁻ rlc1::kanR ade6-M216 leu1-32 ura4.294*	This work
FPR1461	*h? Pcp1-GFP:kanR rlc1::kanR Rlc1-GFP::ura4⁺ myo2.E1 ade6-M216 leu1-32*	This work
FPR1498	*h? Pcp1-GFP:kanR rlc1::kanR Rlc1-GFP::ura4⁺ myo2.E1 for3DAD ade6-M216 leu1-32*	This work
	<u>Figure 6</u>	
E888	*h⁺ for3-3xGFP::ura4⁺ sty1-HA6H::ura4⁺ ade6-M216 leu1-32 ura4-D18*	Gomez-Gil *et al.*, 2020
FPR961	*h⁺ Pcp1-GFP:kanR rlc1::kanR Rlc1-GFP::ura4⁺ ade6-M216 leu1-32*	This work
FPR965	*h⁺ Pcp1-GFP:kanR rlc1::kanR Rlc1(S35A)-GFP::ura4⁺ ade6-M216 leu1-32*	This work
FPR1461	*h? Pcp1-GFP:kanR rlc1::kanR Rlc1-GFP::ura4⁺ myo2.E1 ade6-M216 leu1-32*	This work
FPR727	*h⁻ rlc1::kanR rlc1-HA::ura4⁺ ade6-M216 leu1-32*	This work
FPR645	*h⁻ rlc1::kanR ade6-M216 leu1-32 ura4.294*	This work
FPR730	*h⁻ rlc1::kanR rlc1(S35A)-HA::ura4⁺ ade6-M216 leu1-32*	This work
FPR1489	*h? rlc1::kanR rlc1-HA::ura4⁺ myo2.E1 ade6-M216 leu1-32*	This work
FPR1142	*h? pak1M460G-2xMyc-GFP::ura4⁺ rlc1::kanR shk2::kanR rlc1-HA::ura4⁺ ade6-M216 leu1-32*	This work
FPR1130	*h? rlc1::kanR rlc1-HA::ura4⁺ for3::natR ade6-M216 leu1-32*	This work
FPR1135	*h? rlc1::kanR rlc1(S35A)-HA::ura4⁺ for3::natR ade6-M216 leu1-32*	This work
	<u>Supplementary Figure 1</u>	

MM1	*h+ ade6-M216 leu1-32 ura4.D18*	Madrid *et al.,* 2006
FPR727	*h- rlc1::kanR rlc1-HA::ura4+ ade6-M216 leu1-32*	This work
FPR719	*h- rlc1::kanR pZ3EVrlc1-HA::ura4+ adh1-Z3EV:leu1+ ade6-M216*	This work
FPR722	*h- rlc1::kanR pZ3EVrlc1-HA::ura4+ adh1-Z3EV:leu1+ ade6-M216*	This work
FPR645	*h- rlc1::kanR ade6-M216 leu1-32 ura4.294*	This work
Supplementary Figure 2		
FPR1153	*h? rlc1::kanR rlc1-HA::ura4+ shk1::natR shk1(M460A)::hphR ade6-M216 leu1-32*	This work
PPG4.69	*h+ pak1-GFP::kanR leu1-32 ura4.D18*	Lab stock
FPR1530	*h- shk2::hphR prompak1+shk2-GFP::ura4+ ade6-M216 leu1-32*	This work
Supplementary Figure 3		
FPR961	*h+ Pcp1-GFP:kanR rlc1::kanR Rlc1-GFP::ura4+ ade6-M216 leu1-32*	This work
FPR1126	*h? Pcp1-GFP:kanR rlc1::kanR Rlc1-GFP::ura4+ for3::natR ade6-M216 leu1-32*	This work
FPR965	*h+ Pcp1-GFP:kanR rlc1::kanR Rlc1(S35A)-GFP::ura4+ ade6-M216 leu1-32*	This work
FPR1132	*h? Pcp1-GFP:kanR rlc1::kanR Rlc1(S35A)-GFP::ura4+ for3::natR ade6-M216 leu1-32*	This work
FPR727	*h- rlc1::kanR rlc1-HA::ura4+ ade6-M216 leu1-32*	This work
FPR645	*h- rlc1::kanR ade6-M216 leu1-32 ura4.294*	This work
FPR730	*h- rlc1::kanR rlc1(S35A)-HA::ura4+ ade6-M216 leu1-32*	This work
FPR1130	*h? rlc1::kanR rlc1-HA::ura4+ for3::natR ade6-M216 leu1-32*	This work
FPR1135	*h? rlc1::kanR rlc1(S35A)-HA::ura4+ for3::natR ade6-M216 leu1-32*	This work
E880	*h+ for3-3xGFP::ura4+ ade6-M216 leu1-32 ura4-D18*	Gomez-Gil *et al.,* 2020
E998	*h? for3-3xGFP::ura4+ mts3-1 ade6-M216 leu1-32 ura4-D18*	Gomez-Gil *et al.,* 2020
Supplementary Figure 4		
E32	*h- CRIB-GFP::ura4+ 1 ade6-M216 leu1-32*	Lab Stock
Supplementary Figure 5		
FPR961	*h+ Pcp1-GFP:kanR rlc1::kanR Rlc1-GFP::ura4+ ade6-M216 leu1-32*	This work
FPR1547	*h- Pcp1-GFP:kanR rlc1::kanR Rlc1-GFP::ura4+ myo3::kanR ade6-M216 leu1-32*	This work
FPR965	*h+ Pcp1-GFP:kanR rlc1::kanR Rlc1(S35A)-GFP::ura4+ ade6-M216 leu1-32*	This work
FPR1619	*h? Pcp1-GFP:kanR rlc1::kanR Rlc1(S35A)-GFP::ura4+ myo3::kanR ade6-M216 leu1-32*	This work

27
28

Table S2. Oligonucleotides and DNA fragments used in this study.

OLIGONUCLEOTIDE	SEQUENCE 5'-3'	Use
Rlc1D-FWD	AGTTTTTTTCATTTCTTAATTCTTCCGTACTTTACTTTACAG CATAACTATATCTTATTTGATCATTTGCTCTGTTAACG CGGATCCCCGGGGTTAATTAA	*rlc1⁺* deletion
Rlc1D-REV	TTCGTCTAAGGGAAATGGCTCAGGTTAAAAAGATAAAGTA TTAGAGGGAAGAATGTGAAACATATCTGGCTGCTCTTAAC GAATTCGAGCTCGTTTAAAC	*rlc1⁺* deletion
Rlc1D-COMP FWD	ATCCTCGCCTTACGGTGTATAA	Confirmation of *rlc1⁺* deletion
KAN-COMP-R	GATGTGAGAACTGTATCCTAGCAAG	Confirmation of gene tagging
Rlc1-Seq1-FWD	CTGAGACTTACCAAGAGCTTGAATATC	*rlc1⁺* sequencing
Rlc1-S35A-FWD	**T TCT CAA AGA GTT GCT GCC CAA GCC GCT AAA CGA GCA GCT TCT GGT GCA TTT GCG CAA CTT ACT TCT TCC CAA ATT CAA G**	Rlc1 serine-35 replaced by alanine (site-directed mutagenesis)
Rlc1-S35A-REV	CTTGAATTTGGGAAGAAGTAAGTTGCGCAAATGCACCAGA AGCTGCTCGTTTAGCGGCTTGGGCAGCAACTCTTTGAGA A	Rlc1 serine-35 replaced by alanine (site-directed mutagenesis)
Rlc1-S36A-FWD	**T TCT CAA AGA GTT GCT GCC CAA GCC GCT AAA CGA GCA TCT GCT GGT GCA TTT GCG CAA CTT ACT TCT TCC CAA ATT CAA G**	Rlc1 serine-36 replaced by alanine (site-directed mutagenesis)
Rlc1-S36A-REV	CTTGAATTTGGGAAGAAGTAAGTTGCGCAAATGCACCAGC AGATGCTCGTTTAGCGGCTTGGGCAGCAACTCTTTGAGAA	Rlc1 serine-36 replaced by alanine (site-directed mutagenesis)
Rlc1-S35AS36A-FWD	**T TCT CAA AGA GTT GCT GCC CAA GCC GCT AAA CGA GCA GCT GCT GGT GCA TTT GCG CAA CTT ACT TCT TCC CAA ATT CAA G**	Rlc1 serine-35 and serine-36 replaced by alanine (site-directed mutagenesis)
Rlc1-S35AS36A-REV	CTTGAATTTGGGAAGAAGTAAGTTGCGCAAATGCACCAGC AGCTGCTCGTTTAGCGGCTTGGGCAGCAACTCTTTGAGA A	Rlc1 serine-35 and serine-36 replaced by alanine (site-directed mutagenesis)
Rlc1 (SmaI)- FWD	TAT ATC CCG GGA TGT TCT CTT CGA AGG AAA ATT CCT	*rlc1⁺* clonning in pZ3Ev plasmid
Rlc1-HA (SacII)-REV	TAT ATC CGC GGT CAT GCA TAG TCC GGG ACG TCA TAG GGA TAG CCA TTG CTA TCT TTT GAC CCA GCA	*rlc1⁺* clonning in pZ3Ev plasmid
PromRlc1(XhoI)-FWD	**TATAACTCGAG**GGTGTGCAAGTTCAGACTC	*rlc1⁺* clonning in Pjk210 plasmid
Rlc1-GFP(SacII)-REV	TATTACCGCGGCAGATCTATATTACCCTG	*rlc1⁺* clonning in Pjk210 plasmid
Pak2-Comp-FWD	TGTAACCAATGTCATGTTCGCT	Confirmation of *pak2⁺* deletion
PromPak2(XhoI)-FWD	ACTTA*CTCGAG*CAGTACTCCCAACTTGTTAGATAATG	*pak2⁺* clonning in Pjk210 plasmid
Pak2GFP(SmaI/XmaI)-REV	ATTAA*CCCGGG*ATT AAT ATG GGT ATT CGC TTT GC	*pak2⁺* clonning in Pjk210 plasmid
GFP1-FWD	tctcgcaaagcgaatacccatattaatccc AGTAAAGGAGAAGAACTTTTCACTGG	GFP-tagging for Pak2-3GFP assembly
GFP1-REV	tcctttactggatctTTTGTATAGTTCATCCATGCCATGTG	GFP-tagging for Pak2-3GFP assembly
GFP2-FWD	gatgaactatacaaaAGATCCAGTAAAGGAGAAGAACTTTTC	GFP-tagging for Pak2-3GFP assembly
GFP2-REV	aagttcttctcctttactgttaattaacccTTTGTATAGTTCATCCATGCCA TGTG	GFP-tagging for Pak2-3GFP assembly
PromPak1-FWD	cgacggtatcgataagcttgatatcgaattcctgcagccc TTTAAAAGTATTTGAGTATAATAAATGAAAATTAG	Assembly of *pak1⁺* promoter Pak2-GFP construct

PromPak1-REV	cctcttacacttaaaagcatAGTAAATAAATTTATTAACGAAAAGGG	Assembly of *pak1+* promoter Pak2-GFP construct
Pak2-GFP-FWD	cgttaataaatttatttactATGCTTTTAAGTGTAAGAGGCGTGC	Assembly of *pak1+* promoter Pak2-GFP construct
Pak2-GFP-REV	caagggagacattccttttaCTATTTGTATAGTTCATCCATGCCATG	Assembly of *pak1+* promoter Pak2-GFP construct
Nmt-TERM-FWD	tggatgaactatacaaatagTAAAAGGAATGTCTCCCTTGCCAGTAC	Assembly of *pak1+* promoter Pak2-GFP construct
Nmt1-TERM-REV	ccaccgcggtggcggccgctctagaactagtggatccccc GCATTACTAATAGAAAGGATTATTTCACTTCTAATTACAC	Assembly of *pak1+* promoter Pak2-GFP construct
Ste11-del-FWD	TTAATTCTAAGAACCGTTTCATTTGTTTTATTTTCTCCCTTA CTTTTACTACAATTTTTATATTTACTCTTCTCTACACACGGA TCCCCGGGTTAATTAA	*ste11+* deletion
Ste11-del-REV	ACAAATCAGCTGCATGCTTTTGTGACGCGTTAAAAATGAT CGTTTGTTGAAAACAAAGCCATGTTTGCATAGAAATATTTG AATTCGAGCTCGTTTAAAC	*ste11+* deletion
Ste11-comp-FWD	TCACACCAGTTTTTATTCGGTG	Confirmation of *ste11+* deletion
PromSte11-FWD	CATAACATTTCTTTGTTTTT TGCATTCTCTTTATTTATAAATGGGGTTTCTTTATTTATACA TTTGAGCTAAAATGTATA	G replaced by A (site directed mutagenesis) in TRbox1 and 2 sites within *ste11+* promoter
PromSte11-REV	TATACATTTTAGCTCAAATGTATAAATAAAGAAACCCCATT TATAAATAAAGAGAATGCAAAAAACAAAGAAATGTTATG	G replaced by A (site directed mutagenesis) in TRbox1 and 2 sites within *ste11+* promoter
For3-Seq-F	GGCCACACTGAACCAAAGAG	*for3+* sequencing
Myp2-Comp-FWD	GTGCCTAATATCCTGGCAAAAG	Confirmation of *myo3+* deletion
For3-Comp-FWD	CATCACATCTGATACCTGCGTT	Confirmation of *for3+* deletion
Nat-Comp-REV	TTATTGTCAGTACTGATTAGGGGCA	Confirmation of gene tagging

31
32